

## EVALUATION OF BMP2/miRNA CO-EXPRESSION SYSTEMS FOR POTENT THERAPEUTIC EFFICACY IN BONE-TISSUE REGENERATION

T.K. Brenner<sup>1,§</sup>, K. Posa-Markaryan<sup>1,§</sup>, D. Hercher<sup>1,4</sup>, S. Sperger<sup>1,4</sup>, P. Heimel<sup>1,4</sup>, C. Keibl<sup>1</sup>, S. Nürnberger<sup>1,2,3,4</sup>, J. Grillari<sup>1,4,5</sup>, H. Redl<sup>1,4</sup> and A. Hacobian<sup>1,4,\*</sup>

<sup>1</sup>Ludwig Boltzmann Institute for Experimental and Clinical Traumatology/AUVA Research Centre, The Austrian Cluster for Tissue Regeneration, European Institute of Excellence on Tissue Engineering and Regenerative Medicine Research (Expertissues EEIG), Donaueschingenstrasse 13, 1200 Vienna, Austria

<sup>2</sup>Department of Orthopaedics and Trauma-Surgery, Division of Trauma-Surgery, Medical University of Vienna, Währinger Gürtel 18-20, 1090 Vienna, Austria

<sup>3</sup>University Clinic of Dentistry, Medical University of Vienna, Sensengasse 2a, 1090 Vienna, Austria

<sup>4</sup>Austrian Cluster for Tissue Engineering

<sup>5</sup>Institute for Molecular Biotechnology, Department of Biotechnology, BOKU – University of Natural Resources and Life Sciences, Vienna, Austria

<sup>§</sup>These authors contributed equally to this work

### Abstract

Reconstruction of bone defects and compensation of deficient repair mechanisms represent important goals within the field of regenerative medicine and require novel safe strategies for translation into the clinic. A non-viral osteogenic gene therapeutic vector system ('hybrid vectors') was generated, combining an improved bone morphogenetic protein 2 (*BMP2*) gene cassette and single pro-osteogenic microRNAs (miR-148b-3p, miR-20-5p, miR-590b-5p), driven by the U6 promoter. The vectors were tested *in vitro* for their osteogenic differentiation potential in C2C12 and C3H/10T1/2 cell lines, using *BMP2* alone as a control. After confirming *BMP2* expression and miRNA transcription, increased osteogenic differentiation was observed by all hybrid vectors, but most consistently by *BMP2*/miR-590-5p, using alkaline phosphatase enzyme activity assays and osteogenic marker mRNA quantitation, including runt-related transcription factor 2 (*Runx2*), collagen type 1 (*Col1a1*) and osteocalcin. To visualise target mRNAs of the respective miRNAs, next generation sequencing was performed, confirming down-regulation of mRNA targets of the hybrid vectors. Since the hybrid vector consisting of *BMP2* and miR-590-5p showed the largest increase in osteogenic differentiation *in vitro*, this was tested in a mouse ectopic-bone model. Mineralisation was more than with *BMP2* alone.

The present study showed hybrid vectors as a novel non-viral gene therapeutic plasmid system for combining therapeutic effects of recombinant protein expression and miRNA transcription that did not add to the burden of the translation machinery, while improving the therapeutic efficacies. *In vivo* proof-of-principle in the context of bone regeneration suggested that such hybrid vectors will be applicable in a wide array of gene therapeutic strategies.

**Keywords:** Gene therapy, bone morphogenetic protein 2, microRNA-590, microRNA-148b, microRNA-20a, microRNA, ectopic bone, hybrid vector.

**\*Address for correspondence:** Ara Hacobian, Donaueschingenstrasse 13, 1200 Vienna, Austria. Telephone number: +43 6801348411 Email: a.hacobian@gmx.net

**Copyright policy:** This article is distributed in accordance with Creative Commons Attribution Licence (<http://creativecommons.org/licenses/by-sa/4.0/>).

List of Abbreviations		BAMBI	BMP and activin membrane bound inhibitor
ACTR5	actin-related protein 5	BMP2	bone morphogenetic protein 2
Alk-2	activin receptor-like kinase-2	BMPR2	BMP receptor 2
ALP	alkaline phosphatase	cDNA	complementary DNA
ALPL	liver/bone/kidney alkaline phosphatase	COL1A1	collagen type 1
APC	anaphase-promoting complex	CRIM1	cysteine-rich transmembrane BMP regulator 1

ΔCT	delta threshold cycle
DMEM	Dulbecco's modified Eagle's medium
EF1α	translation elongation factor 1 alpha
ELISA	enzyme-linked immunosorbent assay
FCS	foetal calf serum
FGF	fibroblast growth factor
FOP	fibrodysplasia ossificans progressiva
hASCs	human adipose-tissue-derived stromal cells
HE	haematoxylin and eosin
hMSCs	human mesenchymal stem cells
HPRT	hypoxanthine-guanine phosphoribosyl transferase
hsa-miR	homo sapiens microRNA
μCT	micro-computed tomography
MetLuc	<i>Metridia longa</i> luciferase
miRNA	microRNA
mRNA	messenger RNA
MSCs	mesenchymal stem cells
NGS	next generation sequencing
OCN	osteocalcin
PPARG	peroxisome-proliferator-activated receptor γ
rhBMP2	recombinant human BMP2 protein
rRNA	ribosomal RNA
ROCK1	rho-associated coiled-coil containing protein kinase 1
ROI	region of interest
RT-qPCR	reverse transcription quantitative polymerase chain reaction
RUNX2	runt-related transcription factor 2
SD	standard deviation
shRNA	short hairpin RNA
siRNA	short interfering RNA
SMAD7	SMAD family member 7
snRNA	small nuclear RNA
TGFβ	transforming growth factor β
TGFBR2	TGFβ receptor 2
WNT3A	Wnt family member 3A

## Introduction

Reconstruction of bone defects and compensation for deficient repair mechanisms represent important goals within the field of regenerative medicine. Large bone regeneration is required in complex clinical conditions, such as reconstruction of large bone-defects caused by trauma, infection and tumour resection, or cases in which the regenerative process is compromised, including non-union bone defects and osteoporosis (Audigé *et al.*, 2005; Dimitriou *et al.*, 2011). Current strategies for stimulating bone growth range from application of recombinant protein to viral as well as non-viral gene therapeutic approaches (Bleiziffer *et al.*, 2007; Feichtinger *et al.*, 2014a; Kempen *et al.*, 2010; Koh *et al.*, 2008; Sood *et al.*, 2012; Southwood *et al.*, 2004). Due to transient expression profiles and clinical safety, non-viral

plasmids represent a suitable strategy for clinical translation within tissue regenerative gene therapy (Bleiziffer *et al.*, 2007; Glover *et al.*, 2005).

An improved osteogenic vector system encoding BMP2 was recently introduced (Hacobian *et al.*, 2016). The main bottle-neck of non-viral gene therapy – low target-gene expression – was compensated for by use of a strong promoter, codon optimisation and insertion of an artificial largely truncated intron sequence, resulting in an improved therapeutic BMP2 vector (BMP2-Advanced, in the following referred to as pBMP2<sub>ADV</sub>) (Hacobian *et al.*, 2016). Aside from the need to increase therapeutic protein production, further improvement of therapeutic vector bio-efficacy, such as the simultaneous knockdown of transgene inhibitors, is considered to support successful translation of non-viral vectors to the clinic (Al-Dosari and Gao, 2009; Kay, 2011; Mingozi and High, 2011; Wang *et al.*, 2013). Recently, the application of miRNAs in tissue regeneration has attracted much interest (Peng *et al.*, 2015). At the same time, scientific knowledge of the involvement of miRNAs throughout the osteogenic differentiation cascade (Lian *et al.*, 2012; Zhai *et al.*, 2017) and in bone formation and osteoporosis (*et al.*, 2015a) has increased. In general, miRNA-function can be divided into two categories depending on the degree of sequence complementarity: specific downregulation of target mRNA transcription and/or translation. One mRNA can be regulated by multiple miRNAs just as a single miRNA can recognise a multitude of different targets at once (Lim *et al.*, 2005). Utilisation of miRNAs for *in vivo* bone tissue engineering has recently emerged to specifically enhance or suppress differentiation and target-gene expression (Deng *et al.*, 2014; Eskildsen *et al.*, 2011; Li *et al.*, 2017; Liao *et al.*, 2014). Therefore, a combinatorial approach of miRNA-dependent gene regulation and overexpression of a therapeutic gene encoded by a single-plasmid-system (hybrid vector) has the potential to increase biological efficacy of therapeutic plasmids and drive cellular fate in a desired direction.

Following a literature search, multiple miRNAs potentially involved in the osteogenic pathway were selected for integration into the non-viral pBMP2<sub>ADV</sub> vector. In preliminary tests (data not shown), the selection was reduced to the three most potent candidates, human miR-148b-3p, hsa-miR-590-5p and hsa-miR-20a-5p. These miRNAs were individually incorporated into pBMP2<sub>ADV</sub> under the control of a human U6 promoter, a well-studied competent RNA polymerase III promoter that constitutively transcribes small RNAs (Duvoisin *et al.*, 2012). Combination of these elements resulted in the generation the hybrid plasmids. Then, these plasmids were tested for their osteoinductive potential, *in vitro* as well as *in vivo*, using an ectopic-bone mouse model. The study hypothesis was that these newly designed miRNA-BMP2 co-expression constructs possessed a

greater osteoinductive potency than the previously introduced BMP2 overexpression plasmid (Hacobian *et al.*, 2016).

## Materials and Methods

### Plasmid construction

The BMP2<sub>ADV</sub>-Hybrid vectors (Fig. 1a) include a codon-optimised human BMP2 sequence (Gene ID: 650) with an implemented intron, as previously described (Hacobian *et al.*, 2016). The original EF1 $\alpha$ -BMP2-Adv vector, in the following called pBMP2<sub>ADV</sub> was modified by incorporating a selection of shRNA sequences (Table 1) into the variable cloning site in forward direction respect to the EF-1 $\alpha$  promoter, as this facilitated stronger target gene knockdown (Fig. 1b). A U6 RNA polymerase III promoter was inserted upstream of the shRNAs.

A schematic illustration of control plasmid pHybrid\_MetLuc, specifically designed to investigate miRNA influence on differentiation processes uncoupled from BMP2<sub>ADV</sub> expression, is also depicted in Fig. 1a. BMP2<sub>ADV</sub> was replaced by secreted MetLuc gene.

To investigate successful knockdown of a reporter gene *via* the incorporated shRNA/U6 promoter system, an artificial hairpin structure (anti-Luc) was expressed, targeted against a click-beetle luciferase gene, co-expressed from a pGL3 plasmid (Promega).

### Cell culture and reagents

C3H/10T1/2 (ATCC CCL-226) mouse embryonic cells and Chinese hamster ovary (CHO-K1) cell line (ATCC CCL-61) were cultured in DMEM (Sigma-Aldrich) high glucose (4.5 g/L glucose), supplemented with 2 mmol/L L-glutamine (Sigma-Aldrich) and 10 % FCS (Sigma-Aldrich). C2C12 mouse muscle myoblast

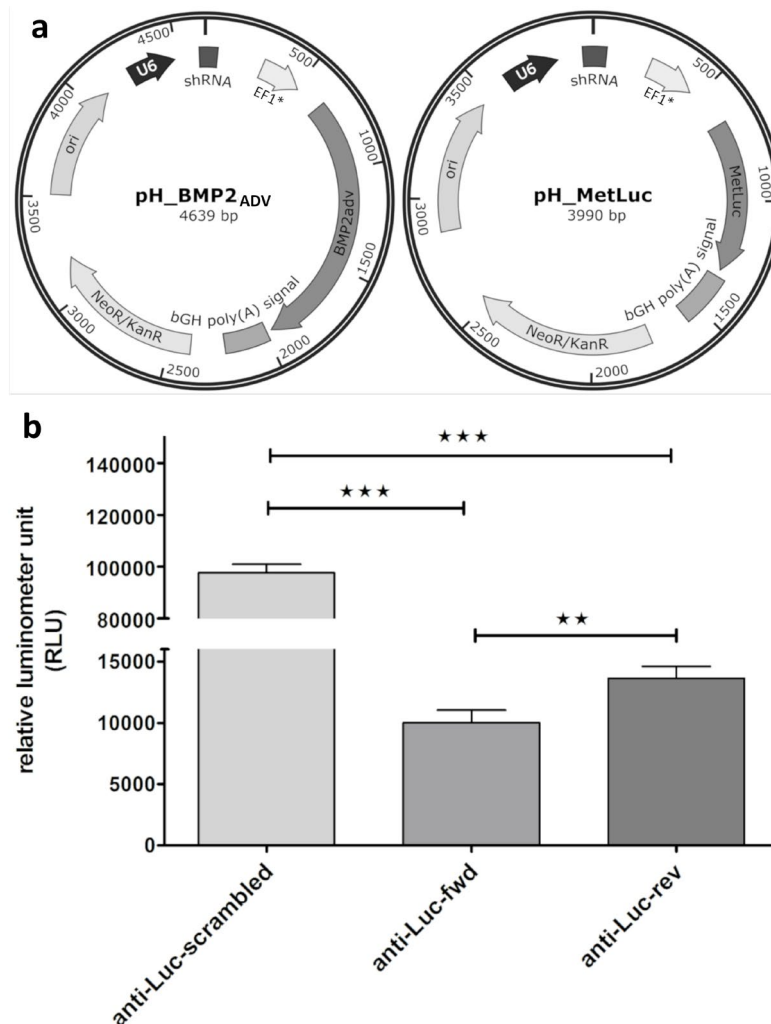


**Fig. 1. Plasmid maps and reporter gene knockdown.** (a) Schematic representation of the Hybrid vector system. U6 RNA III promoter controls shRNA expression. Downstream transcription of a gene of interest, here BMP2<sub>ADV</sub> or *Metridia longa* luciferase, is regulated *via* a minimal EF1 $\alpha$  promoter sequence. Res, antibiotic resistance selection marker; ori, origin of bacterial replication. Plasmid map was designed with SnapGene Viewer software (from GSL Biotech; available at [www.snapgene.com](http://www.snapgene.com)). (b) Reporter luciferase gene knockdown. Luciferase activity 2 d after transfection of C3H/10T1/2 cells. Both anti-Luc hairpin orientations showed successful reduction in target protein. However, forward orientation suppressed luciferase production more efficiently. Averaged data are presented as means  $\pm$  SD,  $n = 8$ . Statistical differences were determined by one-way ANOVA followed by Tukey *post-hoc* test analysis.

**Table 1. List of plasmids constructed and used.**

Plasmid name	Encoded miRNA	NCBI accession number	shRNA sequence (5'-3')
pH_BMP2 <sub>ADV</sub> 148b	hsa-miR-148b	NR_029894.1	CAAGCACGATTAGCATTGAGGTGAAGTTCTGTTATACTCAGGCTGTG-GCTCTCTGAAAGTCAGTGCATCACAGAACTTGTCTCGAAAGCTTTCTA
pH_BMP2 <sub>ADV</sub> 590	hsa-miR-590	NR_030321.1	TAGCCAGTCAGAAATGAGCTTATTCATAAAAAGTGCAGTATGGTGAAGT-CAATCTGTAATTTTATGTATAAGCTAGTCTCTGATTGAAACATGCAGCA
pH_BMP2 <sub>ADV</sub> 20a	hsa-miR-20a	NR_029492.1	GTAGACTAAAAGTGCTTATAGTGCAGGTAGTGTTTAGTTATCTACTGCAT-TATGAGCACTTAAAGTACTGC
pH_BMP2 <sub>ADV</sub> scr	anti-Luc-fwd	n/a	CCCCgactaaactgagcgtccagttTCAAGAGaactggagcgtcagtttagtcTTTT

**Table 2. Primer sequences used for RT-qPCR analysis.**

Target mRNA	NCBI accession number	Forward primer (5'-3')	Reverse primer (5'-3')	Amplicon length	Annealing temperature
BMP2 <sub>ADV</sub>	n/a	GAGCAGATGCAGGATGC	TCCATCTCATCACGGCA	187 bp	61 °C
HPRT	NM_013556.2	AGTCCCAGCGTCGTGATTAG	TGGCCTCCCATCTCCTTCAT	167 bp	63.5 °C
GAPDH	XM_017321385.1	CTGAGTATGTCTGGAGTC	GGATGCATTGCTGACAATC	179 bp	55 °C
ACTR5	XM_016964770	TGCTGGATGCCTGGTATGG	ACCCAGGCTCCACTGTCTTCT	67 bp	62 °C
ALPL	XM_006538497	GCACCTGCCTTACCAACTCTT	GGTACATTGGTGTGAGCTTTT	122 bp	61 °C
COL1A1	XM_021213774	CAGCCGCAAAGAGTCTACATG	GGTTCCACGTCTCACCATTG	172 bp	61 °C
OCN	NM_007541.3	GAACAGACAAGTCCCACACAG	CTGCTTGGACATGAAGGCTTT	448 bp	60 °C
RUNX2	XM_006523540.2	CAAGTAGCCAGGTCAACGA	CTGAGGCGATCAGAGAACAA	209 bp	58 °C

precursor cell line (DSMZ, Braunschweig, Germany, #ACC565) was cultivated under the same conditions except for a reduced serum concentration of 5 %.

#### ***In vitro* transfection**

Cells were seeded 24 h before transfection into 24- or 48-well cell culture plates at a cell density of  $0.25 \times 10^5/\text{cm}^2$  (C3H/10T1/2),  $0.3 \times 10^5/\text{cm}^2$  (C2C12) or  $0.4 \times 10^5/\text{cm}^2$  (CHO-K1). According to the manufacturer's instructions, endotoxin-free plasmids were incubated with transfection reagent (Turbofect, Peqlab Biotechnologie GmbH, Erlangen, Germany) in serum-free medium for 15 min. Target cells were transfected at 80 to 90 % confluency with 1  $\mu\text{g}$  of indicated plasmid/mL medium using 2  $\mu\text{L}$  transfection reagent. 6 h post transfection, medium was changed. Transfection efficiencies were approximated for each cell line using parallel control transfections with GFP-expression plasmids (data not shown). Transfection efficiency was accepted when a level of approximately  $\geq 80$  % was reached. No statistical comparison between cell lines was performed. Therefore, possible differences in transfection efficiency were not considered relevant.

#### **ALP assay**

Transfected cells were lysed for 1 h at room temperature using 100  $\mu\text{L}$  lysis buffer consisting of ALP buffer [0.5 mol/L 2-amino-2-methyl-1-propanol (Sigma-Aldrich, #A9199), 2 mmol/L magnesium chloride (Sigma-Aldrich, #M8266, pH 10.3), 0.5 % Triton X-100 (Sigma-Aldrich, #93443)]. Enzymatic activity was induced by addition of substrate solution, consisting of 20 mmol/L p-nitrophenylphosphate

(Sigma-Aldrich, #71768) in 50  $\mu\text{L}$  ALP buffer. After 20 min, the reaction was stopped using 50  $\mu\text{L}$  of 0.2 mol/L NaOH (Sigma-Aldrich, #71689). Conversion of p-nitrophenylphosphate to p-nitrophenol by ALP was measured at 405 nm using a Polarstar Omega plate reader (BMG Labtech, Ortenberg, Germany). Due to distinct differentiation kinetics, ALP activity was measured 3 (C2C12) and 6 d (C3H/10T1/2) after transfection, respectively. A single treatment with 150 ng/ $\mu\text{L}$  rhBMP2 was used as a positive osteogenic-differentiation control.

#### **Luciferase assay**

Luciferase activity was quantified according to the Renilla Luciferase Assay System (Promega Corporation, #E2810) standard protocol.

#### **ELISA**

Quantification of secreted BMP2 levels was carried out using the DuoSet ELISA Development kit (R&D Systems, #DY335) for human BMP2, according to the manufacturer's instructions. Absorbance was measured at 450 nm using a Polarstar Omega plate reader (BMG Labtech), with wavelength correction at 570 nm. ELISA was performed 2 and 4 d (CHO-K1) as well as 3 and 6 d (C2C12, C3H/10T1/2) after transfection. 100  $\mu\text{L}$  cell culture supernatants were collected at stated time points and cells were incubated in remaining medium up to the last sampling day.

#### **RT-qPCR**

Cells were harvested and total RNA was extracted using TriFast reagent (Peqlab, Biotechnologie

GmbH, #30-2010). Time points for qPCR analysis were selected specifically for each marker of osteogenesis. RNA concentrations were determined using a NanoDrop One spectrophotometer (Thermo Fisher Scientific). cDNA was synthesised from total RNA (2 µg) using an OneScript cDNA Synthesis Kit (abmGood, Richmond, Canada, #G234). Each PCR reaction consisted of 4 µL diluted cDNA (40 ng), 10 µL PerfeCTa SYBR Green SuperMix (Quantabio, Beverly, MA, USA, #733-1247) and specific primer pairs (250 nmol/L) in a total volume of 20 µL. Reaction volume was collected in a colourless PCR 96-well TW-MT plate (Biozym, Hamburg, Germany, #712240X) sealed with adhesive clear PCR seal sheets (Biozym, #600208). Three-step reaction protocols were performed using a C1000/CFX96 Thermal Cycler (BioRad). To confirm amplification specificity, the PCR products were subjected to a dissociation curve analysis. Gene expression levels were reported relative to gene expression of reference gene using the  $2^{-\Delta\Delta Ct}$  method (Schmittgen and Livak, 2008). The reference genes *Hprt* for C2C12 and C3H/10T1/2 (Masilamani *et al.*, 2014; Rahim *et al.*, 2017) and *Actr5* for CHO-K1 (Bahr *et al.*, 2009) were used for normalisation. All primers were synthesised by Microsynth (Balgach, Switzerland). Primer names and sequences used for RT-qPCR are listed in Table 2.

#### miRNA quantification using RT-qPCR

Following C3H/10T1/2 cell transfection with hybrid plasmids, quantification of basal as well as overexpressed cytosolic and secreted miRNAs was conducted by TAmiRNA (Vienna, Austria).

Total RNA was extracted from cell pellets and supernatants using the miRNeasy mini Kit (Qiagen). Samples were thawed on ice and centrifuged at 12,000 ×g for 5 min to remove any cellular debris. For each sample, 200 µL of supernatant or cell pellet were homogenised with 1 mL QIAzol (Qiagen). A mix of three synthetic spike-in controls (Exiqon) was added to QIAzol prior to homogenisation to monitor extraction efficiency and the variance of the analytical procedure. Following incubation at room temperature for 10 min, 200 µL of chloroform were added to the lysates followed by centrifugation at 12,000 ×g for 15 min at 4 °C. 650 µL of the upper aqueous phase were mixed with 7 µL glycogen (50 mg/mL) to enhance precipitation. Samples were transferred to a miRNeasy mini column and RNA was precipitated using 750 µL ethanol followed by automated washing with RPE and RWT buffer in a QiaCube liquid handling robot. Finally, total RNA was eluted in 30 µL nuclease-free water and stored at -80 °C until further analysis.

Starting from total RNA samples, cDNA was synthesised using the Universal cDNA Synthesis Kit II (Exiqon). Reaction conditions were set according to recommendations by the manufacturer. For total RNA extracted from supernatants, 2 µL of total RNA were used per 10 µL reverse transcription reaction, since RNA concentrations were below the

limit of detection. In contrast, 10 ng total RNA from cell pellets were applied for reverse transcription. PCR amplification was performed in a 96-well plate using a Roche LC480 II instrument and EXiLENT SYBR Green master mix (Exiqon), with the following settings: 95 °C for 10 min, 45 cycles of 95 °C for 10 s and 60 °C for 60 s, followed by melting curve analysis. The second derivative maximum method was used to calculate the cycle of quantification values (Ct-values).

In case of supernatants, the raw Ct-values were normalised to the RNA spike-in control level, by subtracting the individual miRNA Ct-value from the individual RNA Spike-In Ct, thus obtaining delta Ct ( $\Delta Ct$ ) values that were used for the analysis. In case of cell pellets, U6 snRNA and 5S rRNA (assays derived from Exiqon) of each sample were used for individual normalisation using the same procedure.

#### NGS

Total RNA from C3H/10T1/2 cell lysate was collected 3 d after transfection. mRNA libraries were generated from 100 ng total RNA input using Quant Seq 3'mRNA Library Prep KitFWD for Illumina (Lexogen, Austria) according to the manufacturer's instructions. Libraries were amplified for 16 cycles using barcoded Illumina reverse primer (i7 index primer) in combination with Illumina forward primer. Fragment size and quantity was assessed using the Bioanalyzer DNA High Sensitivity Chip (Agilent). An equimolar pool was generated from the individual libraries and sequenced on an Illumina HiSeq2500 with 100 bp single-end reads.

#### NGS data analysis

Reads obtained by NGS were analysed using the integrated Data Analysis Pipeline on the Bluebee® platform. This pipeline uses fastQC (v0.11.5) (Web ref. 1) for overall sequencing quality assessment and bbdutk (v35.92) to trim adapters and polyA tails. Reads are aligned with the STAR aligner (v2.5.2a) (Dobin *et al.*, 2013) and gene reads counted using HTSeq-count (v0.6.0) (Anders *et al.*, 2015). Differential expression analysis is performed with DESeq2 (v3.11) (Love *et al.*, 2014) following best practice guidelines from the package's description. Validated miRNA-targets for mmu-miR-20a-5p, mmu-miR-148b-3p and mmu-miR-590-5p were obtained from TarBase (Karagkouni *et al.*, 2018). As the seed sequences of mmu-miR-590-5p and mmu-miR-21-5p are identical, the latter's targets were also included.

#### In vivo transfection

Eight female CD-1® mice [Charles River, Crl:CD1 (ICR)], 14 weeks old and weighing approximately 30 g were used in the ectopic-bone model. Mouse analgesia was performed using Meloxicam (0.1 mg/kg, Boehringer Ingelheim). Prior to transfection, mice were placed under inhalation anaesthesia with isoflurane 1 to 3 volume % (Forane, AbbVie, Vienna, Austria) and 3 L/min air. 30 µg of plasmid DNA was

first incubated for 20 min at room temperature with *In vivo* PolyMag™ Transfection Reagent (OzBiosciences, Marseille, France, #IV-PN31000) at a 1 : 2 ratio for complex formation in a total volume of 100  $\mu$ L. Subsequently, complexed DNA was injected in a single-shot manner into the centre of the *musculus gastrocnemius* at the hind limb using a 27G needle. Magnets (17  $\times$  17  $\times$  5 mm) were applied at the site of transfection for 30 min to facilitate gene delivery. Animal experiments were approved by the City Government of Vienna, Austria and were conducted in accordance with the Guide for the Care and Use of Laboratory Animals as defined by the National Institute of Health (TVA-No.: 1755694/2014/11).

### $\mu$ CT

All 16 hind limbs were scanned 8 weeks after transfection and hind limb harvested using a SCANCO  $\mu$ CT 50 (SCANCO AG) at 70 kVp, 200  $\mu$ A with an integration time of 500 ms. The resulting resolution was 10  $\mu$ m isotropic. Calcification volumes were measured using ImageJ 1.51h, Fiji (Eliceiri *et al.*, 2012; Schindelin *et al.*, 2012). A ROI that included all visible ectopic calcifications was drawn using the ROI Manager. A minimal gap of 150  $\mu$ m was kept between the entopic bone and the ROI. Scans were median-filtered using the 3D median filter with a radius of 3 pixels. The volume of all structures inside the ROI above a threshold of 100 mgHA/cm<sup>3</sup> was measured.

### Histological analysis

After an 8-week observation period, all mice were euthanised by cervical dislocation under inhalation anaesthesia using isoflurane 5 volume % (Forane, AbbVie) and 3 L/min air. Hind limbs were removed as proximally as possible, fixed for 48 h in 4 % formaldehyde solution, rinsed in tap water,

transferred to 50 % ethanol for slow dehydration of samples and stored in 70 % ethanol at 4 °C. *Musculus gastrocnemius* was excised and embedded in paraffin-wax using a Tissue-Tek VIP (Sakura Finetek Europe, Alphen aan den Rijn, the Netherlands). Multiple sections of each sample were stained with HE, as well as von Kossa and collagen type 2 (NeoMarkers, Fremont, CA, USA, MS-306-P1) for detection of mineralisation, according to standard histological protocols. Samples were processed using a Microm HM 355 s microtome (Thermo Fisher Scientific) to 3  $\mu$ m slices for HE staining and 4  $\mu$ m slices for von Kossa and collagen type 2 staining.

### Statistical analysis

Averaged data are presented as mean  $\pm$  SD. Data sets were tested for Gaussian distribution using Kolmogorov-Smirnov test (with Dallal-Wilkinson-Lillie for *p* value). Subsequent comparison between multiple data groups was performed by one-way ANOVA followed by Tukey or Dunnett *post-hoc* test analysis. All statistical analyses were performed using GraphPad Prism 5 software. Differences were considered statistically significant at \* *p* < 0.05, \*\* *p* < 0.01, \*\*\* *p* < 0.001.

## Results

### Forward orientation of a miRNA-expression cassette was optimised for knockdown of luciferase target example

To validate the most efficient orientation of the miRNA expression cassettes, shRNA expression system plasmids harbouring a shRNA targeting click-beetle luciferase gene, co-expressed from a pGL3 plasmid, were transiently introduced into C3H/10T1/2 cells.

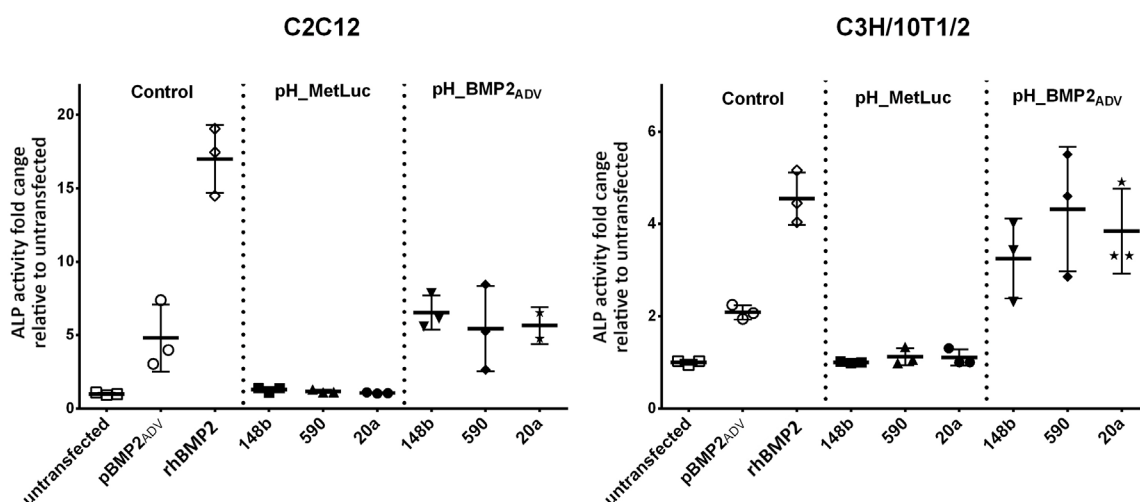


**Fig. 2. ALP activity assay.** ALP enzyme activity in C2C12 and C3H/10T1/2 cells after transfection. pH\_MetLuc control plasmids encoding for *Metridia longa* luciferase and miRNAs, namely pH\_MetLuc148b, pH\_MetLuc590 and pH\_MetLuc20a. pBMP2<sub>ADV</sub> pH\_BMP2<sub>ADV</sub>148b, pH\_BMP2<sub>ADV</sub>590 and pH\_BMP2<sub>ADV</sub>20a were analysed relative to untransfected control. 150 ng/mL rhBMP2 was used as a positive control. Quantification of ALP activity was measured 3 (C2C12) and 6 d (C3H/10T1/2) after transfection. Averaged data are presented as means  $\pm$  SD, *n* = 3.

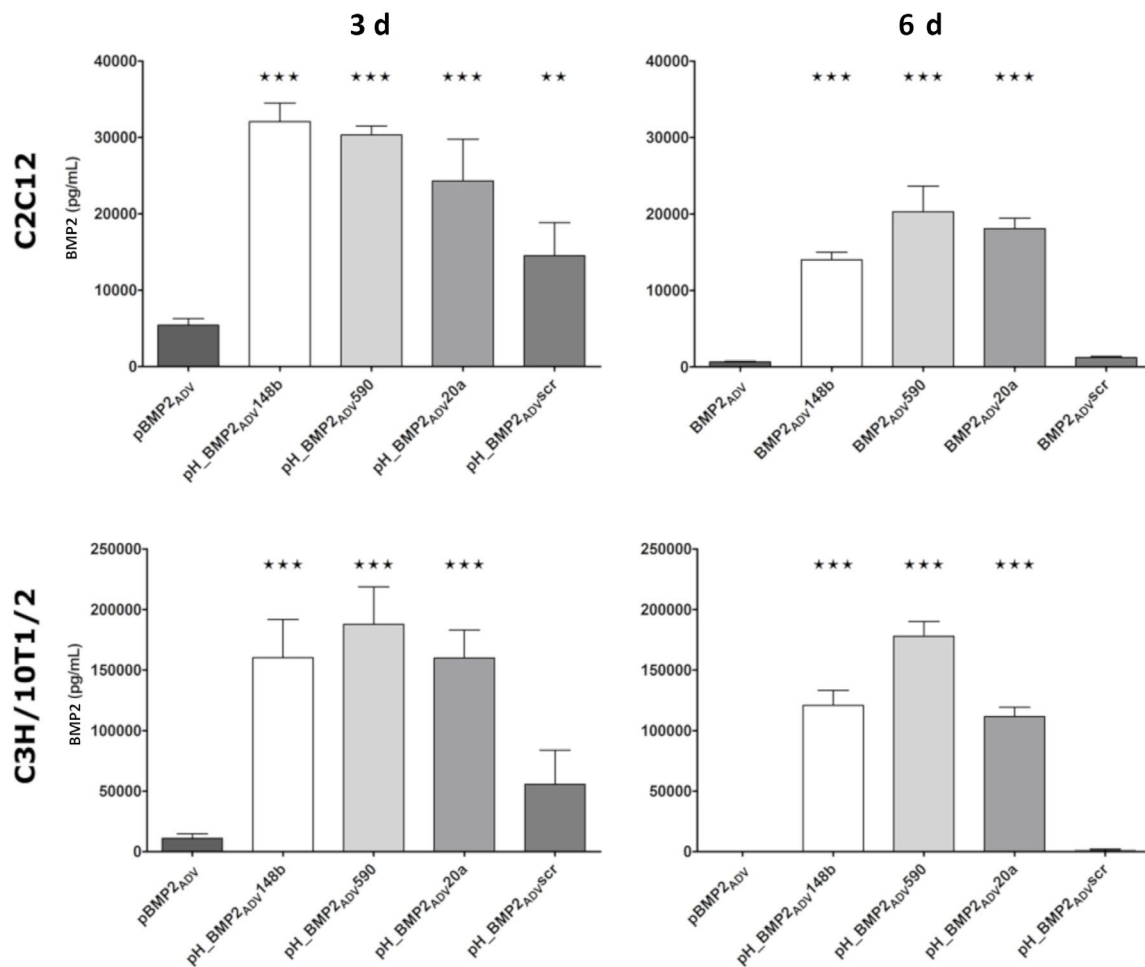


**Fig. 3.** Secreted BMP2 protein levels by C2C12 and C3H/10T1/2 determined by ELISA in cell supernatants after transfection with pH\_BMP2<sub>ADV</sub>148b, pH\_BMP2<sub>ADV</sub>590, pH\_BMP2<sub>ADV</sub>20a, pH\_BMP2<sub>ADV</sub>scr or pBMP2<sub>ADV</sub> plasmids. Supernatants were sampled 3 and 6 d after transfection. Averaged data are presented as means  $\pm$  SD, 3 d  $n = 4$ , 6 d  $n = 3$ . Statistical differences were determined by one-way ANOVA followed by Tukey *post-hoc* test analysis, comparing all groups with control group pBMP2<sub>ADV</sub>.

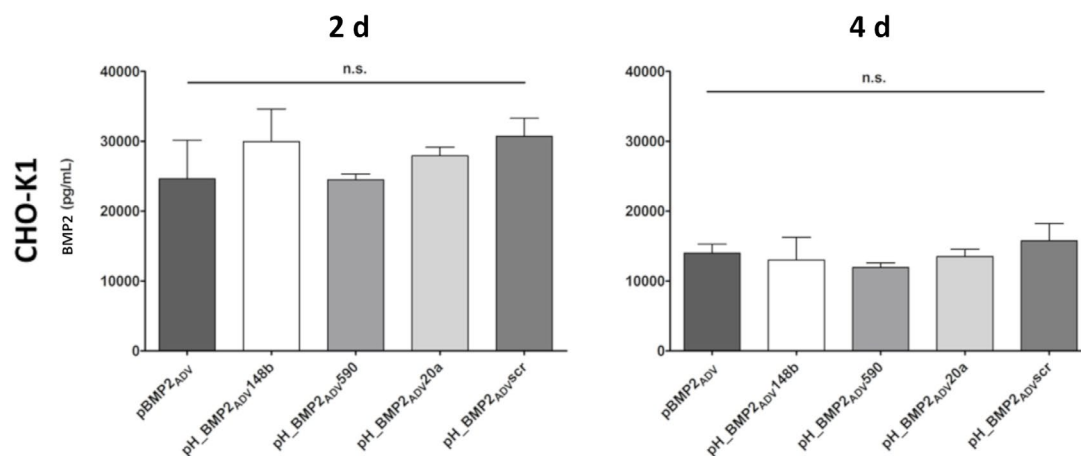


**Fig. 4.** Secreted BMP2 protein levels in CHO-K1 cells; determined by ELISA. Cells were transfected with pH\_BMP2<sub>ADV</sub>148b, pH\_BMP2<sub>ADV</sub>590, pH\_BMP2<sub>ADV</sub>20a, pH\_BMP2<sub>ADV</sub>scr or pBMP2<sub>ADV</sub>. Cell supernatants were sampled 2 and 4 d after transfection. Data are represented as means  $\pm$  SD,  $n = 3$ . Statistical differences were determined by one-way ANOVA followed by Tukey *post-hoc* test analysis.

shRNA was expressed either in sense (convergent) or antisense (divergent) orientation in respect to the EF-1 $\alpha$ -promoter-controlled luciferase expression module. shRNA efficiency in downregulating luciferase activity was quantified through luciferase assay 2 d after transfection. Target enzyme activity was significantly reduced when the anti-Luc miRNA was co-expressed in comparison to the control plasmid [containing a missense hairpin structure instead (scrambled)]. In addition, convergent co-expression of the anti-Luc hairpin (anti-Luc-fwd) resulted in significantly stronger downregulation of target luciferase than divergent co-expression (anti-Luc-rev) (Fig. 1b). Based on these data, a consecutive expression design was adopted for the subsequent construction of the osteogenic hybrid plasmids.

#### miRNAs alone were not able to induce osteogenic differentiation in target cells

To compare the osteogenic potency of miRNAs alone or co-expressed with *BMP2*, a control hybrid vector system, pH\_MetLuc, was constructed expressing osteogenic miRNAs in the absence of

*BMP2*. Transfection of C2C12 and C3H/10T1/2 cells with pH\_MetLuc hybrid plasmids was surprisingly not sufficient to induce osteogenic differentiation (quantified by ALP activity), independent of the used shRNA, while the hybrid vectors did (Fig. 2). rhBMP2 protein treatment (150 ng/ $\mu$ L) resulted in an increase in ALP enzyme. In C2C12, this positive control exceeded the osteogenic effect of hybrid plasmid transfection.

#### Hybrid vectors increased BMP2 protein levels in C2C12 and C3H/10T1/2 cells after transfection

To evaluate the influence of the miRNA expression cassette on the expression level of the adjacent *BMP2* cassette, C2C12 and C3H/10T1/2 cells were transfected with hybrid vectors (Fig. 3) for subsequent quantification of secreted BMP2. To track time-dependent expression changes, supernatants of transfected cells were collected at day 3 and 6. In both studied cell types, the highest BMP2 protein levels were reached when cells were transfected with either pH\_BMP2<sub>ADV</sub>148b, pH\_BMP2<sub>ADV</sub>590 or pH\_BMP2<sub>ADV</sub>20a. The lowest concentration of BMP2

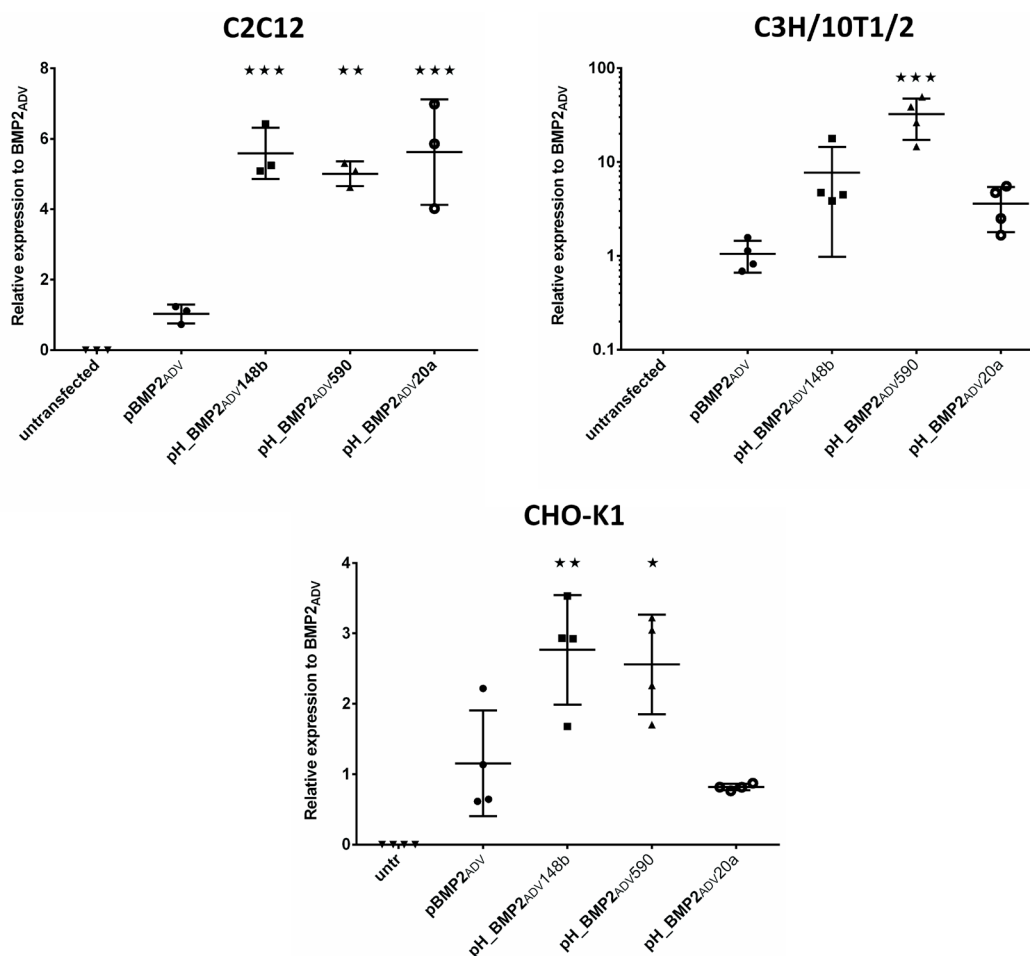


**Fig. 5. RT-qPCR gene expression analysis.** C2C12, C3H/10T1/2 and CHO-K1 cellular mRNA after transfection with pH\_BMP2<sub>ADV</sub>148b, pH\_BMP2<sub>ADV</sub>590, pH\_BMP2<sub>ADV</sub>20a or pBMP2<sub>ADV</sub> plasmid. Quantification of BMP2<sub>ADV</sub> transcript levels was performed 3 d after transfection. Expression data represented as  $\Delta\Delta$ Ct values relative to pBMP2<sub>ADV</sub>. Reference genes *Hprt* (C2C12 and C3H/10T1/2) and *Actr5* (CHO-K1) were used for normalisation. C3H/10T1/2 data are depicted logarithmically. Averaged data are presented as means  $\pm$  SD,  $n \geq 3$ .

protein was detected in supernatants when cells were transfected with pBMP2<sub>ADV</sub>. Only in C2C12 at day 3, pH\_BMP2<sub>ADV</sub>scr showed significantly higher therapeutic protein levels when compared to pBMP2<sub>ADV</sub> which was followed by a strong decrease over the investigated time course.

### Homogeneous expression of BMP2 in CHO-K1 cells upon hybrid vector transfection

To exclude one possible cause for BMP2 variation – BMP2 consumption due to cellular uptake during cell differentiation (Garzon-Alvarado *et al.*, 2014) – osteogenic-differentiation-incompetent CHO-K1 cells were transfected with selected hybrid plasmids. Interestingly, they showed comparable BMP2 expression levels over a 4 d time course (Fig. 4). At day 2 and 4 after transfection, no significant difference between construct groups was detectable.

### Quantification of BMP2<sub>ADV</sub> and miRNA transcription levels and subsequent localisation of miRNAs

To evaluate consistency of gene transcription (mRNA levels) and BMP2 protein production, amounts of BMP2<sub>ADV</sub> mRNA produced by different hybrid vector constructs (harbouring different miRNAs) were quantified using RT-qPCR (Fig. 5) for subsequent comparison with BMP2 protein levels. Hybrid-vector-generated mRNA levels of BMP2<sub>ADV</sub> significantly exceeded those of pBMP2<sub>ADV</sub> control (conventional plasmid lacking miRNA expression cassette). In CHO-K1 cells, pH\_BMP2<sub>ADV</sub>148b and pH\_BMP2<sub>ADV</sub>590 induced the largest amounts of BMP2<sub>ADV</sub> mRNA, whereas pH\_BMP2<sub>ADV</sub>20a and pBMP2<sub>ADV</sub> reached similar relative expression levels. In C2C12 cells, all hybrid constructs displayed significantly larger amounts of BMP2<sub>ADV</sub> mRNA than pBMP2<sub>ADV</sub> control. Interestingly, C3H/10T1/2 cells transfected with pH\_BMP2<sub>ADV</sub>590 resulted in significantly higher transgene mRNA expression when compared with

other hybrid plasmid constructs harbouring other miRNA sequences. Untransfected cells served as a negative control, lacking a primer-specific transcript.

To verify miRNAs' overexpression, determine their intracellular *versus* secreted levels and understand their potential paracrine effects, C3H/10T1/2 cells were transfected with the chosen hybrid vector constructs. pBMP2<sub>ADV</sub> plasmid transfection served as normalisation sample for osteogenic expression of miRNAs 20a-5p, 148b-3p and 590-5p. Intracellular and extracellular miRNA levels were analysed (Fig. 6), always comparing miRNA transcript levels after transfection with the plasmid expressing the same miRNA. Baseline miRNA levels were similar intracellularly and extracellularly (data not shown). In comparison to cells transfected with pBMP2<sub>ADV</sub> a 57.0 ± 5.3-fold increase of miR-148b-3p expression levels was detected intracellularly, while an 80.2 ± 30.1-fold increase was observed in extracellular supernatants. Elevated expression levels were also observed for miRNAs 20a-5p and 590-5p after corresponding hybrid plasmid transfection. Abundance of miR-20a-5p increased intracellularly by 1.9 ± 0.1 and extracellularly by 1.9 ± 0.7-fold. Expression level of miR-590-5p changed 18.0 ± 9.6-fold upon transfection intracellularly and 5.3 ± 2.1-fold in extracellular supernatant samples. Secretion of these miRNAs into body fluids has indeed been observed in the context of bone metabolism and dysfunctions (*et al.*, 2013; Zhang *et al.*, 2020).

### miRNA590 exhibited the highest potential for osteoinduction in C2C12 and C3H/10T1/2 cells

Biomarkers for osteoinduction, *Alpl*, *Col1a1*, *Runx2* and *OCN*, were found to be differentially up-regulated in C2C12 and C3H/10T1/2 cells after transfection with hybrid constructs (Fig. 7). In C3H/10T1/2 cells, pH\_BMP2<sub>ADV</sub>148b, pH\_BMP2<sub>ADV</sub>590 and pH\_BMP2<sub>ADV</sub>20a reached significantly higher levels of *OCN* mRNA

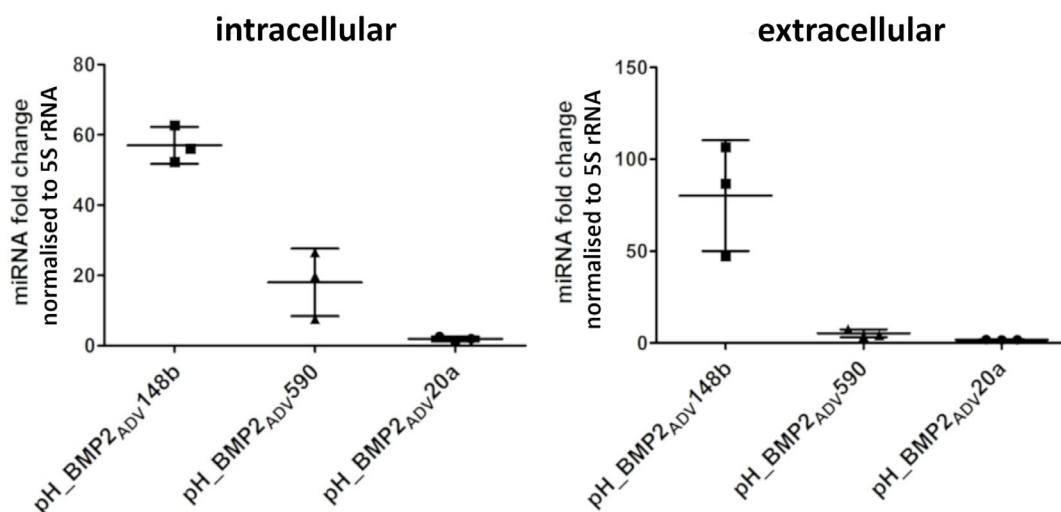


**Fig. 6. Intracellular and extracellular miRNA localisation profiles 2 d after transfection of C3H/10T1/2 cells.** Data were normalised to reference genes U6 snRNA, 5S rRNA (intracellular) and RNA Spike-In (extracellular) and are presented relative to pBMP2<sub>ADV</sub> transfection (vector lacking miRNA expression cassette) as means ± SD, *n* = 3.

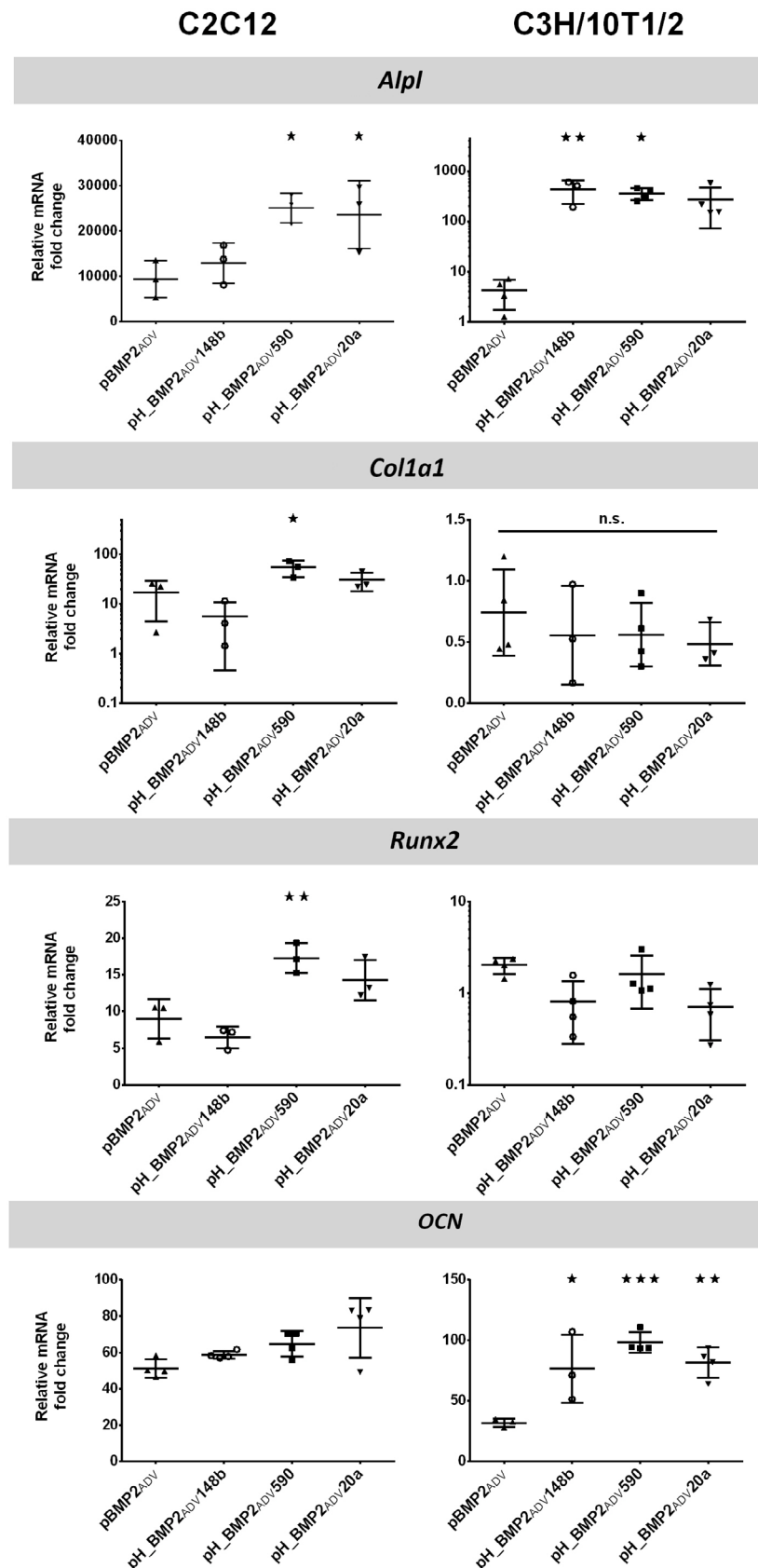


**Fig. 7.** RT-qPCR analysis of C2C12 and C3H/10T1/2 cell lines. Cells were transfected with pH\_BMP2<sub>ADV</sub>148b, pH\_BMP2<sub>ADV</sub>590, pH\_BMP2<sub>ADV</sub>20a or pBMP2<sub>ADV</sub> plasmid. Total RNA was collected 3 (C2C12) and 6 d (C3H/10T1/2) after transfection. Threshold cycles (Ct) of each reaction, relative to untransfected control group, were normalised to those obtained for reference mRNA using  $2^{-\Delta\Delta C_t}$  method. Individual data sets are depicted in a logarithmic scale. Statistical differences were determined by one-way ANOVA followed by Tukey *post-hoc* test analysis, comparing all groups with pBMP2<sub>ADV</sub>. Averaged data are presented as means  $\pm$  SD,  $n \geq 3$ .

when compared with conventional pBMP2<sub>ADV</sub> plasmid. All 3 hybrid vectors led to significantly increased OCN mRNA counts. No difference in *Col1a1* mRNA expression was detected between transfected groups and untransfected control. In C2C12, *Alpl* mRNA was up-regulated in all transfected cells, especially pH\_BMP2<sub>ADV</sub>590 and pH\_BMP2<sub>ADV</sub>20a led to a significantly larger mRNA increase. In addition, *Runx2* mRNA levels were up-regulated the most in C2C12 cells transfected with pH\_BMP2<sub>ADV</sub>590 and pH\_BMP2<sub>ADV</sub>20a. *Col1a1* expression significantly increased upon transfection with pH\_BMP2<sub>ADV</sub>590. mRNA levels were quantified 3 (C2C12) and 6 d (C3H/10T1/2) after transfection.

### Regulation of mRNAs after hybrid vector transfection suggested miRNA-specific mRNA targets

To confirm that the 3 miRNAs showed specific patterns of mRNA regulation, NGS of mRNAs was performed 3 d after transfecting C3H/10T/1 cells with pH\_BMP2<sub>ADV</sub>20a, pH\_BMP2<sub>ADV</sub>148b, pH\_BMP2<sub>ADV</sub>590 and pBMP2<sub>ADV</sub> plasmid. All hybrid RNA profile data were analysed relative to pBMP2<sub>ADV</sub> serving as control. To exclude effects of BMP2 alone, the mRNA transcription profiles were compared to pBMP2<sub>ADV</sub>. NGS data were controlled for total and mapped reads. Raw data were submitted to GEO (Web ref. 2) (accession number GSE166110). Principal component analysis showed clustering of the 3 independent transfections, whereby pBMP2<sub>ADV</sub>590 hybrid was more distinct than the others (Fig. 8a). Transfection of cells with pH\_BMP2<sub>ADV</sub>590 resulted in identification of 532 significantly up-regulated and 463 significantly down-regulated genes. While pH\_BMP2<sub>ADV</sub>20a resulted in an up-regulation of 78 and a down-regulation of 100 genes, transfection with pH\_BMP2<sub>ADV</sub>148b showed 68 genes to be up-regulated significantly and 32 genes to be down-

regulated significantly. Fig. 8b shows the number of significantly up-regulated and Fig. 8c down-regulated genes after hybrid vector *versus* BMP2<sub>ADV</sub> only transfection. Overlapping areas represent significantly affected genes common to all 3 hybrid vectors (Table 3,4). Since all 3 hybrid constructs resulted in increased osteogenic differentiation *in vitro*, this could be reflected in the small number of jointly regulated mRNAs, which might be indispensable for boosting osteogenesis and on which the very specific and different regulatory activity of the 3 different miRNAs converge. Such a specific activity of the single miRNAs is supported by the fact that the differentially expressed mRNAs after miR-590, 20a and 148b are prevailing.

To corroborate specific effects of the 3 single miRNAs, the study hypothesis was that confirmed target mRNAs would be down-regulated after transfection. Therefore, the significantly down-regulated mRNAs were compared to the complete list of validated specific miRNA targets derived from TarBase (Karagkouni *et al.*, 2018) (Fig. 9). Indeed, of all significantly down-regulated genes after transfection with pH\_BMP2<sub>ADV</sub>590, 134 (28.57 %) were validated targets (Fig. 9a). For pH\_BMP2<sub>ADV</sub>20a, a lower fraction of 23 mRNAs (23.00 %) of total significantly down-regulated genes was matched with validated targets (Fig. 9b). pH\_BMP2<sub>ADV</sub>148b led to the down-regulation of 2 validated targets, which was 6.25 % of all significantly down-regulated genes affected by this plasmid (Fig. 9c). Summarised, these data prompted the selection of the BMP2/miR-590-5p hybrid vector for an *in vivo* proof-of-principle study.

### *In vivo* transfection of pH\_BMP2<sub>ADV</sub>590 indicated osteogenic potential of hybrid plasmid

pH\_BMP2<sub>ADV</sub>590, as one of the most promising plasmids regarding osteoinductive potential *in vitro*, was directly compared to the original pBMP2<sub>ADV</sub>

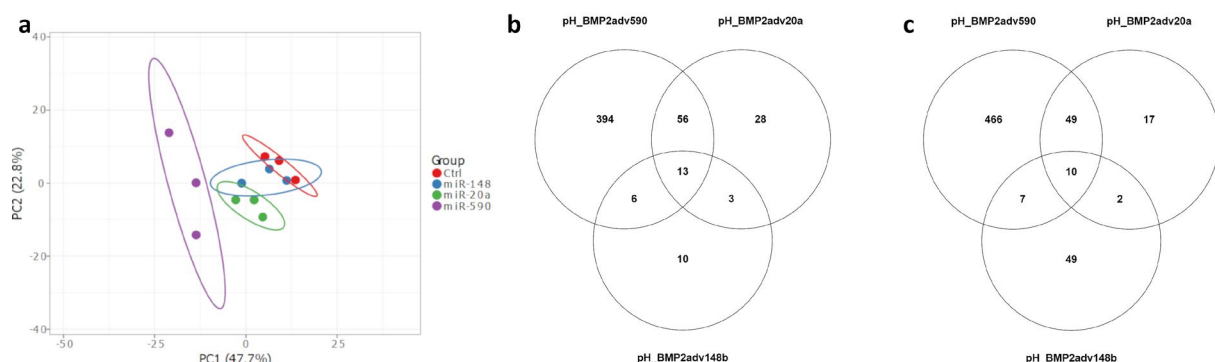


**Fig. 8. NGS principle components analysis and commonly regulated genes.** (a) Principal component analysis of NGS data showed clustering of the 3 independent transfections of C3H/10T/1 cells with either pH\_BMP2<sub>ADV</sub>148b, pH\_BMP2<sub>ADV</sub>20a or pH\_BMP2<sub>ADV</sub>590, whereby pBMP2<sub>ADV</sub>590 hybrid was more distinct than the others. NGS was used to identify significantly (b) down- and (c) up-regulated genes 3 d after transfection of C3H/10T/1 cells with either pH\_BMP2<sub>ADV</sub>148b, pH\_BMP2<sub>ADV</sub>20a or pH\_BMP2<sub>ADV</sub>590. Generated data were calculated relative to transfection of C3H/10T/1 cells with pBMP2<sub>ADV</sub>. Overlapping areas indicate the number of commonly regulated genes, with 13 targets significantly down- and 10 targets significantly up-regulated in all three transfection settings.

**Table 3. List of 13 common significantly down-regulated genes.**

Abbreviated gene name	Full gene name	Ensemble code
<i>Gadd45b</i>	Growth arrest and DNA-damage-inducible 45 beta	ENSMUSG00000015312
<i>Resf1</i>	Retroelement silencing factor 1	ENSMUSG00000032712
<i>Klf6</i>	Kruppel-like factor 6	ENSMUSG00000000078
<i>Rnd1</i>	Rho family GTPase 1	ENSMUSG00000054855
<i>Csf1</i>	Colony stimulating factor 1	ENSMUSG00000014599
<i>Mt2</i>	Metallothionein 2	ENSMUSG00000031762
<i>Adamts5</i>	A disintegrin-like and metallopeptidase (reprolysin type) with thrombospondin type 1 motif, 5	ENSMUSG00000022894
<i>2610008E11Rik</i>	RIKEN cDNA 2610008E11 gene	ENSMUSG00000060301
<i>Gadd45g</i>	Growth arrest and DNA-damage-inducible 45 gamma	ENSMUSG00000021453
<i>Ajuba</i>	Ajuba LIM protein	ENSMUSG00000022178
<i>SnhG15</i>	Small nucleolar RNA host gene 15	ENSMUSG00000085156
<i>Ccl2</i>	Chemokine (C-C motif) ligand 2	ENSMUSG00000035385
<i>2410006H16Rik</i>	RIKEN cDNA 2410006H16 gene	ENSMUSG00000086841

**Table 4. List of 10 common significantly up-regulated genes.**

Abbreviated gene name	Full gene name	Ensemble
<i>Rpl41</i>	Ribosomal protein L41	ENSMUSG00000093674
<i>Myl6</i>	Myosin, light polypeptide 6, alkali, smooth muscle and non-muscle	ENSMUSG00000090841
<i>Adgrg2</i>	Adhesion G protein-coupled receptor G2	ENSMUSG00000031298
<i>Rgs2</i>	Regulator of G-protein signaling 2	ENSMUSG00000026360
<i>Mmp2</i>	Matrix metalloproteinase 2	ENSMUSG00000031740
<i>Hey1</i>	Hairy/enhancer-of-split related with YRPW motif 1	ENSMUSG00000040289
<i>Pass</i>	Prosaposin/Spingolipid activator protein	ENSMUSG00000004207
<i>Krt13</i>	Kreatin 13	ENSMUSG00000044041
<i>Cdsn</i>	Corneodesmosin	ENSMUSG00000039518
<i>Mmp11</i>	Matrix metalloproteinase 11	ENSMUSG0000000901

plasmid in an *in vivo* ectopic-bone mouse model. To allow for optimal intra-animal comparison, each hind limb was transfected with one of the plasmids. 8 weeks after transfection, hind limbs were scanned *ex vivo* for ectopic mineralisation by high-resolution computed tomography (Fig. 10). None of the 4 transfections with the negative control luciferase plasmid showed relevant mineralisation (Fig. 10c). In all animals but one, mineralised volumes were larger when transfected with the hybrid plasmid instead of the original pBMP2<sub>ADV</sub>. Four out of 6 *in vivo* muscle transfections with pH<sub>BMP2<sub>ADV</sub></sub>590, but only 1 out of 6 pBMP2<sub>ADV</sub> transfections, showed significant mineralisation (Fig. 11). Ectopic-bone volume varied strongly and showed substantial differences in shape.

#### Histological analysis confirmed ectopic mineralisation

Histological evaluation of transfected muscle tissue sites, 8 weeks after plasmid injection, confirmed formation of mineralisation in accordance with  $\mu$ CT images. Upon standard HE and von Kossa treatment, muscle tissue transfected with pBMP2<sub>ADV</sub> and pH<sub>BMP2<sub>ADV</sub></sub>590 hybrid plasmid revealed mineralised

areas (Fig. 12,13). Collagen type 2-enriched matrix was shown by positive immunostaining within the area of interest (brown). In contrast, transfection with luciferase control plasmid did not induce intramuscular mineralisation. Response differences to transfection with the same plasmid were visible in histology. While pBMP2<sub>ADV</sub> #1 showed extensive mineralisation within the muscle tissue, the other hind limb transfected with pBMP2<sub>ADV</sub> #2 showed distinctly less mineralisation. Similarly, the variability in osteoinduction of the same plasmids became apparent in histological images of pH<sub>BMP2<sub>ADV</sub></sub>590 #1, #2 and #3, where #3 revealed the smallest area of mineralisation.

#### Discussion

Recent developments in terms of miRNA expression profiles and subsequent target silencing within the setting of tissue regeneration offer an additional approach to enhance the biological impact of non-viral gene therapy. The main objective of the present study was to utilise miRNA gene-regulation

to further increase the efficacy of the previously published osteogenic vector system (Hacobian *et al.*, 2016). This was accomplished by combining an optimised BMP2 ( $BMP2_{ADV}$ ) under the control of an EF1 $\alpha$  minimal promoter with different shRNA sequences regulated by a human RNA polymerase III U6 promoter. In a previous study, Hacobian *et al.* (2016) showed that the EF1 $\alpha$  promoter regulation is superior to the CMV promoter in terms of expression level and duration. The U6 promoter was chosen due to its well-studied, competent and constitutive small-RNA-transcription properties (Duvoisin *et al.*, 2012).

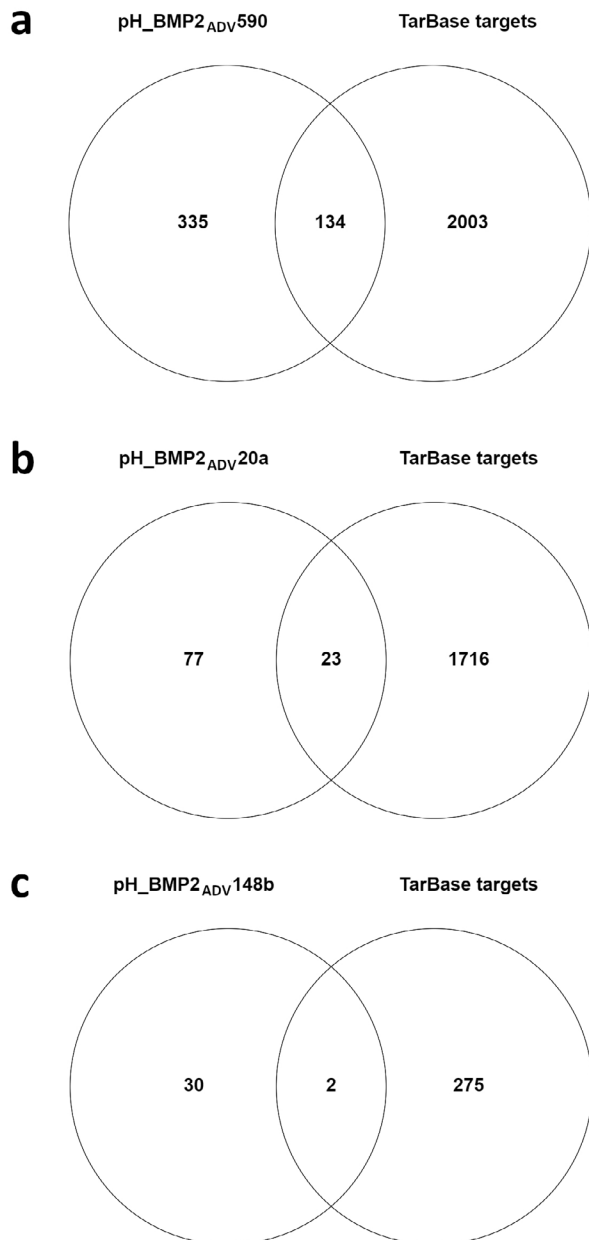


**Fig. 9. Identified miRNA-targets versus validated targets.** The diagram depicts the significantly down-regulated genes 3 d after transfection of C3H/10T/1 cells with (a) pH\_BMP2<sub>ADV</sub>590, (b) pH\_BMP2<sub>ADV</sub>20a, or (c) pH\_BMP2<sub>ADV</sub>148b, identified by NGS and mapped against all miRNA-specific validated targets derived from TarBase (Karagkouni *et al.*, 2018).

To validate the miRNA expression system, luciferase-reporter gene activity was down-regulated *via* expression of a specific anti-Luc shRNA from a co-transfected plasmid. When comparing forward and reverse orientation (with regard to the co-expressed luciferase transgene) of the U6 promoter anti-Luc hairpin expression cassette, significantly more reduction in luciferase protein expression was facilitated by the forward expression direction (Fig. 1b). The existence of the promoter interference phenomena has been described before (Shearwin *et al.*, 2005), such as for a constitutive CMV-promoter co-expression system (Feichtinger *et al.*, 2014a). There, transgene co-expression from the same plasmid lead to lower protein levels when compared to the expression from two distinct plasmids, indicating a negative cross talk between the RNA polymerase II promoters. On the other hand, the present study indicated a positive influence of synchronic polymerase II and III promoter activity. Therefore, the synchronous rather than the asynchronous or bidirectional arrangement of expression units was adopted for the osteogenic hybrid plasmids.

To test the hybrid system in an osteogenic set-up, 3 candidate miRNAs (hsa-miR-148b-3p, hsa-miR-590-5p, hsa-miR-20a-5p) and a control scrambled anti-Luc miRNA were selected for further experiments and incorporated into the hybrid vector system (Fig. 1). To evaluate the isolated osteogenic potential of each miRNA, hybrid plasmids were tested against control plasmids pH\_MetLuc, which expressed *Metridia longa* luciferase instead of  $BMP2_{ADV}$ . Keeping the expression occurrence of reporter gene and shRNA constant, whilst excluding influence of the growth factor was not sufficient to increase ALP enzyme activity in C2C12 and C3H/10T1/2 cell lines at the selected time points (Fig. 2). The murine myoblast cell line C2C12 was chosen as an *in vitro* osteogenic transdifferentiation model, due to its rapid cellular response following BMP2 treatment and the functional resemblance to the *in vivo* experimental setup, where mouse muscle tissue was transfected. To test the plasmids in a non-osteogenic multipotent cell line, C3H/10T1/2 cells were also used for *in vitro* transfection experiments. Albeit miR-148b-3p alone can result in differentiation of hASCs into an osteogenic lineage (Qureshi *et al.*, 2013), it was not possible to confirm this effect at selected time points in the experiments using C2C12 and C3H/10T1/2 cell lines. A possible explanation may be a prolonged processing time and a lower overall concentration of active miR-148b-3p, when introduced *via* transient gene expression as compared to transfection with particle-conjugated pre-processed single stranded miR-148b-3p (Qureshi *et al.*, 2013). The early ALP assay sampling time point (3 d) for C2C12 was based on the observation of myogenic changes in morphology, which are thought to be irreversible, as early as 4 d after transfection (data not shown), if no BMP2 transgene was co-introduced. At the designated time points, C2C12 as well as C3H/10T1/2

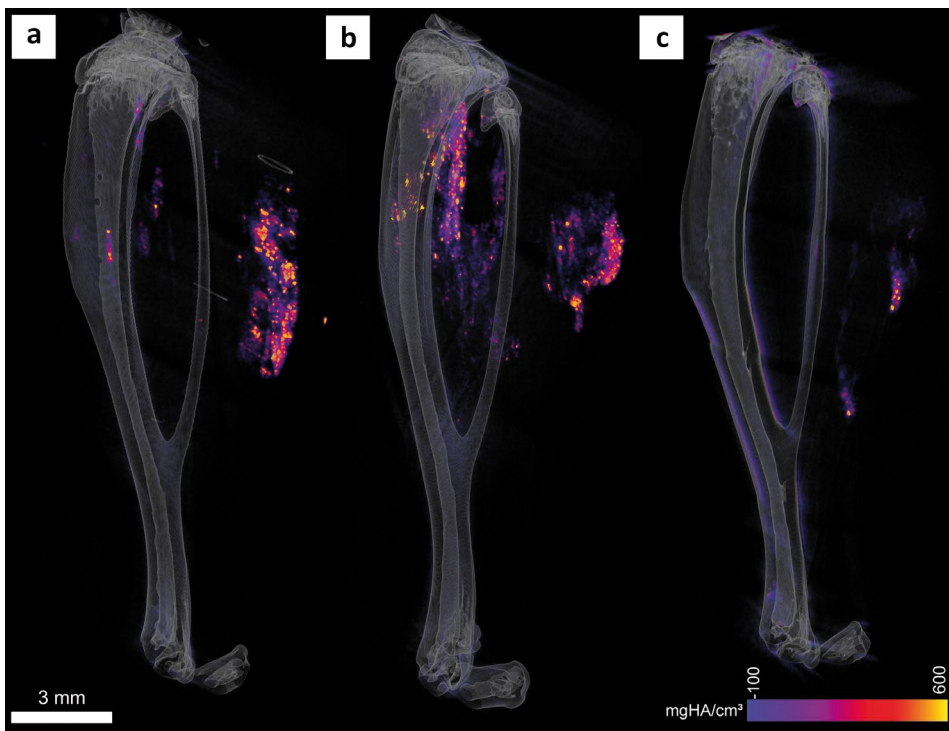


**Fig. 10. Representative  $\mu$ CT-images of mouse hind limbs 8 weeks after transfection.** Coloured areas indicate mineralisation. Changes of shading, from violet to yellow, increase with density. Bones (tibia and fibula) are visualised in grey. (a) pBMP2<sub>ADV</sub>; (b) pH\_BMP2<sub>ADV</sub>590; (c) luciferase control plasmid.

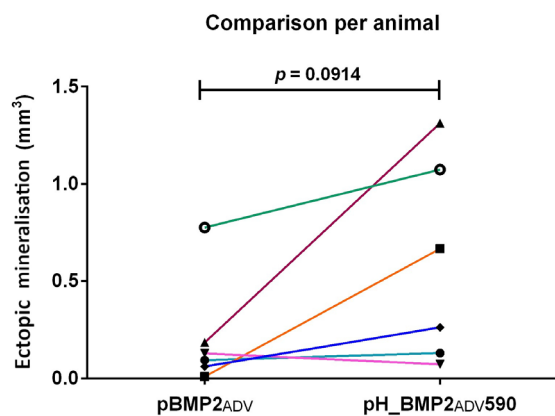


**Fig. 11. Intra-animal comparison of ectopic mineralised volumes.** Each line represents a single animal and each dot the limb harbouring the tested plasmid.

cells (6 d time point) showed strong induction of ALP enzyme activity when treated with rhBMP2 protein (150 ng/mL). Although pBMP<sub>ADV</sub> induced an increase in ALP activity, compared to the pH\_MetLuc group, this difference was not statistically significant. C3H/10T1/2 showed a delayed induction of differentiation as compared to C2C12. Therefore, a later sampling time point for ALP assay was chosen.

Interestingly, ELISA showed that BMP2 protein amounts produced by cells transfected with different hybrid vectors differed significantly between studied cell types (C2C12 and C3H/10T1/2) (Fig. 3). The detected protein was a combination of endogenous and transgenic Bmp2, as these are not distinguishable by their amino-acid sequence. The obtained results may be affected by enhanced endogenous protein production by simultaneously introduced miRNA

(positive feedback loop of Bmp2 production). One of hsa-miR-148b-3p's targets predicted by the miRTargetLink free online software tool (Hamberg *et al.*, 2016) was *Rock1*, which when inhibited has been shown to increase transcription factor Runx2 nuclear translocation as well as differentiation and mineralisation of rat calvarial osteoblasts (Prowse *et al.*, 2013), demonstrating the pro-osteogenic properties of miR-148b-3p. miR-148b-3p affects osteogenic differentiation of hMSCs in a positive manner, as verified by increased ALP enzyme activity (Schoolmeesters *et al.*, 2009). Furthermore, in hASCs, baculovirus-mediated expression of the same miRNA improves osteogenesis *in vitro* and implantation of hASCs co-expressing BMP2/miR-148b-3p accelerates as well as ameliorates bone healing and remodelling in a critical-size calvarial defect model (Liao *et al.*, 2014). Target prediction of hsa-miR-20a-5p revealed incongruent results. On one hand, *Bmpr2* and *Tgfb2*, both important for BMP2-mediated cellular signalling, were supposedly down-regulated. Therefore, reduced osteogenic differentiation would be expected. On the other hand, the same non-coding RNA knocks-down BMP2 antagonists *Crim1*, *BAMBI* as well as *PPARG* (Wilkinson *et al.*, 2003; Umulis *et al.*, 2009; Zhang *et al.*, 2011). Measurement of knockdown efficacy of these targets might give more insight into the hsa-miR-20a-5p mode of action. In the case of hsa-miR-590-5p, strong evidence exists for the targets *TGFBR2* (Ekhteraei-Tousi *et al.*, 2015) and *Smad* (Vishal *et al.*, 2017), a corepressor of *Runx2*. Reduced repression of the transcription factor *RUNX2* enables elevated BMP2-induced osteogenic gene expression. The complementary seed sequence hsa-miR-590-3p induces osteogenic differentiation in MSCs. The underlying mechanism includes knockdown of

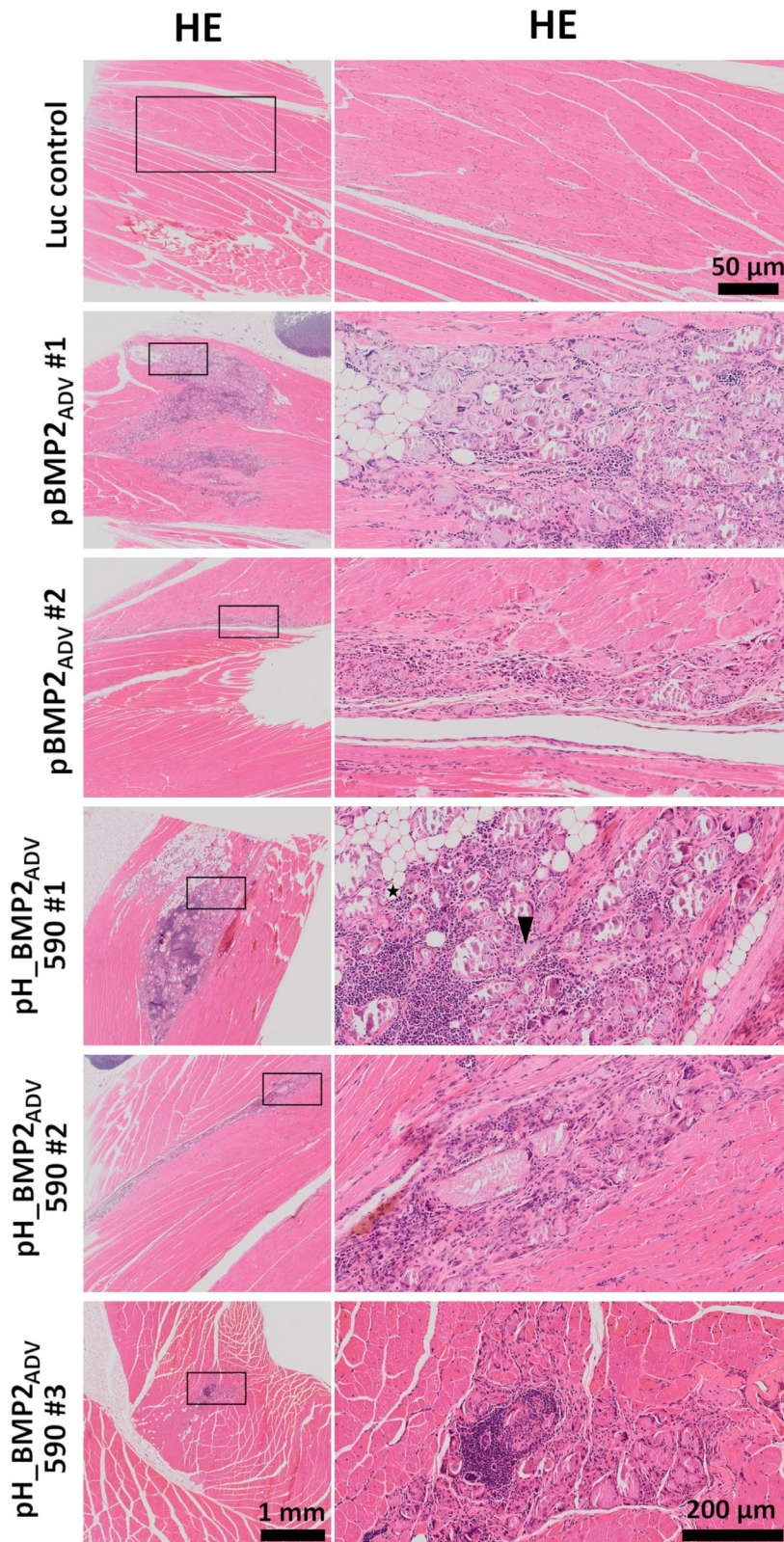


**Fig. 12. Histology of intramuscular mineralisation 8 weeks after plasmid transfection.** Higher magnification in the right column of the area of interest is indicated by a black rectangle in the left column. HE staining of muscle tissue transfected with luciferase control, pBMP2<sub>ADV</sub> or pH\_BMP2<sub>ADV</sub>590. Mineralised ectopic tissue (arrowhead) is indicated by violet, brittle areas embedded within the muscle tissue in the HE staining, blood vessels (not shown) and fatty tissue (star) are also present within the transformed tissue. To underline variability of induced mineralisation, samples representing high and low response to transfection were included, labelled with #1 (high response) and #2 (low response) for the pBMP2<sub>ADV</sub> plasmid. Histological samples pH\_BMP2<sub>ADV</sub>590#1 and pH\_BMP2<sub>ADV</sub>590#2 showed high response, while #3 represented a low response sample upon transfection. Scale bars at the bottom of images account for all images of column except if indicated differently.

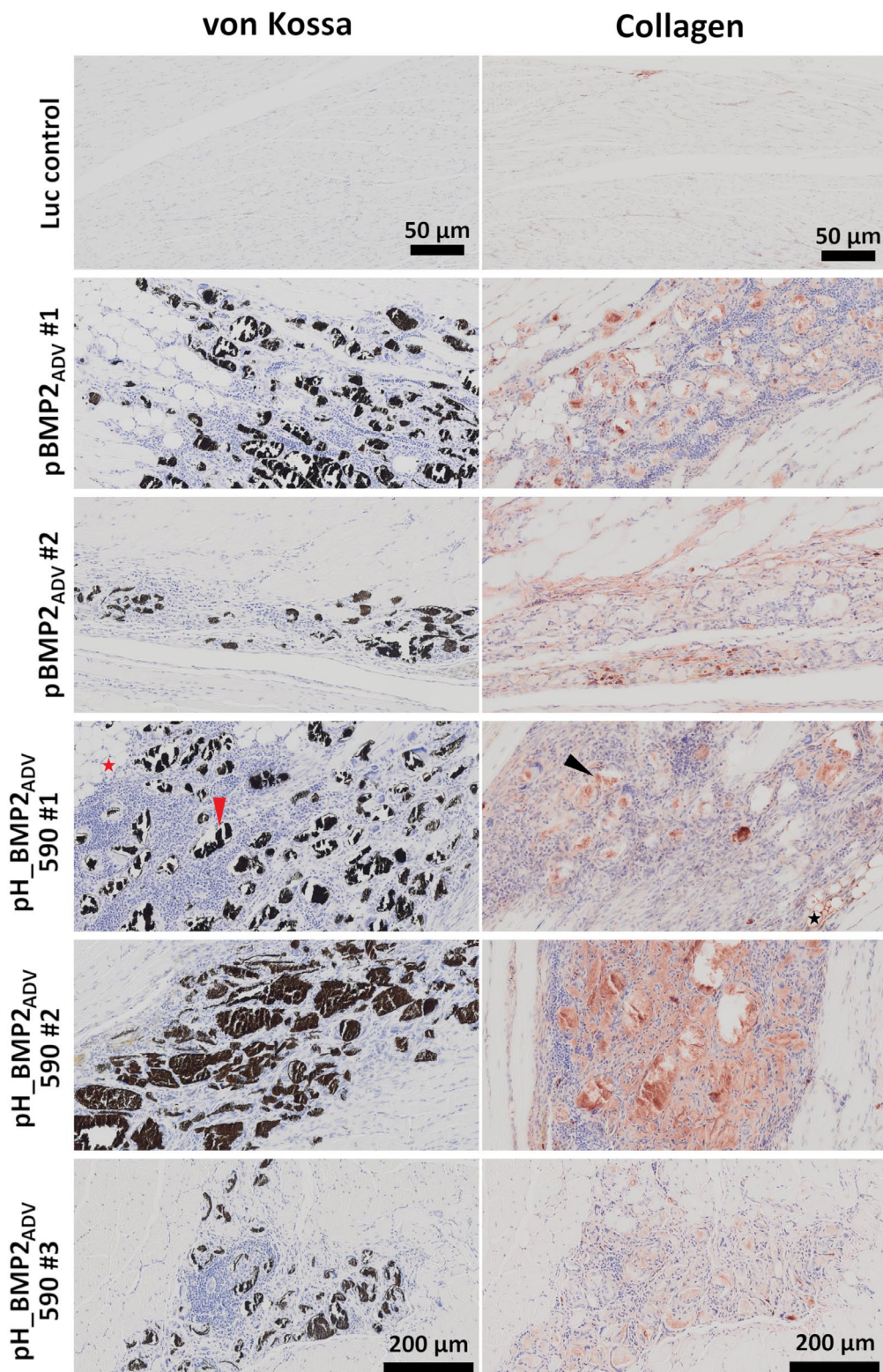


**Fig. 13. Histology of intramuscular mineralisation 8 weeks after plasmid transfection.** The images are the higher magnification of the area of interest as indicated by the black rectangle in Fig. 12, here stained with von Kossa and antibodies against collagen. The muscle tissue was transfected with luciferase control, pBMP2<sub>ADV</sub> or pH\_BMP2<sub>ADV</sub>590. Mineralised ectopic tissue (arrowhead) is indicated by distinctly black areas visible in the von Kossa staining. Collagen type 2-enriched matrix is indicated by brown staining. Blood vessels (not shown) and fatty tissue (star) are also present within the transformed tissue. To underline variability of induced mineralisation, samples representing high and low response to transfection were included, labelled with #1 (high response) and #2 (low response) for the pBMP2<sub>ADV</sub> plasmid. Histological samples pH\_BMP2<sub>ADV</sub>590#1 and pH\_BMP2<sub>ADV</sub>590#2 showed high response, while #3 represented a low response sample upon transfection. Scale bars at the bottom of images account for all images of column except if indicated differently.

APC and consequently activation of Wnt/ $\beta$  catenin signalling (canonical WNT pathway) through stabilisation of Wnt-target gene transcription factor  $\beta$  catenin (Wu *et al.*, 2016).

In C2C12, transfection with pH\_BMP2<sub>ADV</sub>scr resulted in increased Bmp2 protein level detected by ELISA, when compared with pBMP2<sub>ADV</sub> (Fig. 3). As the scrambled miRNA does not specifically bind to any known mRNA, this difference must be facilitated by other interactions. Cross-talk between two promoters in local vicinity can lead to a positive, up-regulatory effect on neighbouring genes (Hampf and Gossen, 2007). This kind of transcriptional influence has been described for promoters of the same type (polymerase II) (Feichtinger *et al.*, 2014a), where the convergent arrangement of expression cassettes had a favourable effect on transgene expression levels when compared to a divergent arrangement. There might be underlying promoter cross-talk events leading to the observed Bmp2 protein up-regulating properties of the U6-miRNA expression machinery.

Quantification of BMP2 protein secreted by CHO-K1 cells transfected with hybrid constructs showed no significant variance between all tested plasmids (Fig. 4). As this cell line has a reduced consumption of produced BMP2 due to its deficiency in osteogenic differentiation (Garzon-Alvarado *et al.*, 2014), the measured BMP2 protein levels could reflect plasmidal expression more directly. Thus, revealing a consistent expression potential of all tested constructs.

Transcription levels of BMP2<sub>ADV</sub> were analysed by RT-qPCR using intron-spanning primers specifically targeting only the codon-optimised version of BMP2. As shown in Fig. 5, mRNA amounts of the introduced therapeutic gene were differing for each hybrid vector as well as between all used cell types 3 d after transfection. In CHO-K1 cells, where protein analysis indicated homogenous expression levels, significant differences in mRNA amounts were detected. In the same cell type, pBMP2<sub>ADV</sub> and pH\_BMP2<sub>ADV</sub>20a constructs resulted in the translation of equal Bmp2 protein amount from lower mRNA counts. This phenomenon may be caused by distinct mRNA abundance, ribosome occupancy and turnover (Maier *et al.*, 2009). In C2C12 cells, all miRNA-encoding vectors achieved significantly larger mRNA counts than the conventional pBMP2<sub>ADV</sub>. This finding was consistent with Bmp2 protein quantification by ELISA (Fig. 3). C3H/10T1/2 cells, on the other hand, only showed significantly enhanced expression of BMP2<sub>ADV</sub> mRNA upon transfection with pH\_BMP2<sub>ADV</sub>590, whereas Bmp2 concentrations in supernatants were similarly enhanced by all hybrid vectors. Thus, overexpression of these miRNAs must influence the translation of transgenic and endogenous Bmp2 protein either directly by stabilising the encoding mRNA or indirectly by repressing the translation of inhibiting factors (Vasudevan, 2012).

The next step was to elucidate if miRNAs were *de facto* overexpressed and if so, to what extent they were

secreted into the extracellular environment enabling a paracrine effect that might be involved in the osteoinductive process within the tissue (Linero and Chaparro, 2014; Santos *et al.*, 2011; Scott *et al.*, 2012). This inquiry was confirmed after quantifying miRNA levels of intracellular and extracellular samples following cell transfection (Fig. 6). Hence, up-regulation of miR-148b-3p and miR-590-5p inside the cell as well as in the supernatant was detected when cells were transfected with corresponding hybrid vectors, relative to cells transfected with pBMP2<sub>ADV</sub> construct. Interestingly, miR-148b-3p displayed the highest up-regulation. This might seem favourable, but as a saturation of miRNA-machinery, *e.g.* exportin-5, can occur, supraphysiological amounts of unprocessed miRNA can be disadvantageous (Grimm *et al.*, 2010). The lower increase in intracellular and extracellular miR-20a-5p, upon hybrid transfection, could be explained by higher endogenous transcript levels in the investigated cell line (data not shown). Thus, the potential relative change is minimised.

miRNAs are reported to regulate many aspects of bone development (Li *et al.*, 2017; Vishal *et al.*, 2017). The present study focused on consequential differentiation of target cells. The evaluation method of choice was RT-qPCR, as it is an acknowledged sensitive transcriptional validation technique and allowed for the study of osteoblast-related genes serving as early and late differentiation markers (Fig. 7). Changes in *OCN* and *Runx2* mRNA after miRNA transfection are reported as early as one night after transfection (Gómez *et al.*, 2013). 3 d after transfection with miR-690, changes in *Alpl* expression are measured (Yu *et al.*, 2016). Huang *et al.* (2014) treated C2C12 with BMP2 protein for 3 d leading to changes in *OCN* and *Col1a1* mRNA. Based on these studies, changes in osteogenic gene expression were tested 3 d after transfection in C2C12 and 6 d after transfection in C3H/10T1/2.

In C2C12, the largest *Alpl* mRNA fold change occurred upon transfection with pH\_BMP2<sub>ADV</sub>590 and pH\_BMP2<sub>ADV</sub>20a. Also, the early markers *Col1a1* and *Runx2* were significantly more up-regulated in the presence of miR-590-5p than upon transfection with pBMP2<sub>ADV</sub> alone. In C2C12, mRNA expression levels of *OCN* were up-regulated the most by pH\_BMP2<sub>ADV</sub>20a transfection. In C3H/10T1/2 cells, pH\_BMP2<sub>ADV</sub>148b and pH\_BMP2<sub>ADV</sub>590 hybrid vectors caused a comparably significant fold change of *Alpl* mRNA transcription, whereas relative type I collagen mRNA count was similar in all groups, even in the untransfected control. As *Alpl* is known to be regulated by Wnt3a signalling (Rawadi *et al.*, 2003) in contrast to *Col1a1* (Jackson *et al.*, 2005), a differentially regulated signalling pathway may be the explanation for this inconsistent transcriptional regulation upon transfection. *Runx2* transcription was not positively affected by miRNA co-expression when compared with BMP2<sub>ADV</sub> expression alone. Osteocalcin mRNA quantification indicated an up-regulation in all C3H/10T1/2 cells transfected with hybrid constructs.

Generation of NGS profiles after transfection of C3H/10T/1 with hybrid plasmids revealed regulation of specific and commonly regulated miRNA targets as depicted in Fig. 8b,c. These findings clearly supported the hypothesis that the plasmid's effects on gene regulation and hence expression are driven by the different miRNAs incorporated in the vectors.

While transfection with pH\_BMP2<sub>ADV</sub>590 resulted in the largest number of significantly up- and down-regulated targets, it also showed the largest number of validated miRNA targets extracted from TarBase, which supported its choice for an *in vivo* study. Of note, miR-590 shares seed sequence homology to miR-21-5p (Web ref. 3), which is also well known for its regulatory role in bone metabolism (Strauss *et al.*, 2020; *et al.*, 2015b; Zarecki *et al.*, 2020).

The presented sum of *in vitro* gene expression data supported the hypothesis that a combinatorial approach of BMP2<sub>ADV</sub> and osteogenic miRNA overexpression led to enhanced osteogenic differentiation. Yet, the inability to proof the own inherent osteogenic potential of the used miRNAs (ALP assay), as well as the absence of transfection experiments in primary MSCs might represent the main limitations of the *in vitro* study design. Yet, the preliminary *in vitro* data was considered solid enough to proceed to *in vivo* testing.

A mouse ectopic-bone model was chosen for translating the hybrid plasmid system from cell culture to an *in vivo* setting. As the osteoinductive potential of miR-590-5p was most stable *in vitro*, pH\_BMP2<sub>ADV</sub>590 hybrid vector was selected for direct comparison with the original pBMP2<sub>ADV</sub>. Each hind limb was transfected with one of the plasmids, allowing for intra-animal comparison. Final high-resolution *ex vivo*  $\mu$ CT scans were conducted after 8 weeks.

In 4 out of 6 hind limbs, transfection with the pH\_BMP2<sub>ADV</sub>590 hybrid vector resulted in substantial mineralisation, when compared to the negative control plasmid (Fig. 11). On the other hand, in only 1 out of 6 injected hind limbs, transfection with pBMP2<sub>ADV</sub> plasmid led to mineralisation. The transfection success-rate of the pH\_BMP2<sub>ADV</sub>590 hybrid vector (4 out of 6 limbs, 67%) was comparable to the 2 W sonoporative gene delivery rate of the non-viral BMP2/7 co-expression plasmid constructed by Feichtinger *et al.* (2014b). Although, sonoporation with 4 W resulted in a 100% transfection rate, which is comparable to the viral gene delivery conducted by Luk *et al.* (2003), who also detected ossification in all rats upon injection of AAV-BMP4. On the other hand, in the present study, the plasmid was administered only once by single injection of DNA-complexes, while sonoporation by Feichtinger *et al.* (2014b) was carried out repeatedly for 5 consecutive days. However, when compared to Feichtinger's study, the tissue samples of the present study did not show a stem cell niche.

Although both plasmids were able to induce mineralisation in an ectopic model, the hybrid

vector showed a higher probability of mineralisation occurrence and, therefore, a greater potential for further *in vivo* trials. This may be due to a variety of osteoinductive properties of the miR-590-5p, such as increased *Alpl* expression *via* targeting Smad7, an inhibitor of osteoblast differentiation (Vishal *et al.*, 2017). Accordingly, hsa-miR-590 overexpression increases pro-osteogenic target expression by stabilisation of  $\beta$  catenin in human MSCs (Wu *et al.*, 2016). Confirming previous findings (Chen *et al.*, 2009), extracellular miRNAs was detected in mesenchymal cell supernatants (Fig. 6). Consequently, overexpressed *Bmp2* and miR-590-5p might act not only intracellularly but also intercellularly *via* paracrine effects in transfected muscle tissue.

As outlined by Wosczyzna *et al.* (2012), excess BMP and induction of intracellular effectors such as SMADs contribute to ossification within the muscle tissue. In human FOP, a mutation of the BMP type I receptor (Alk-2) results in hypersensitive or even BMP-independent signalling, leading to ossification of muscle tissue upon soft tissue trauma. Although the detailed pathophysiology of muscle tissue ossification is still unclear, potential explanations for muscle-bone transformation involve recruitment and differentiation of circulating osteoprogenitor cells restricted to the skeletal muscle, such as satellite cells, as well as the contribution of endothelial cells or multipotent mesenchymal cells to the mouse muscle tissue. Concerning bone tissue formation pathways, Lounev *et al.* (2009) showed that endothelial precursor cells can be triggered by an inflammatory microenvironment to differentiate *via* the endochondral pathway in an animal model of FOP. Also, a study using adenoviral vectors (Jane *et al.*, 2002) expressing BMP2 for intramuscular injection, showed ectopic-bone formation by endochondral ossification. In the present study, the presence of collagen type II-enriched matrix surrounding mineralised areas (Fig. 12) in the absence of collagen type I (data not shown) suggested bone formation *via* the endochondral pathway (Stoeger *et al.*, 2002).

The vector system showed great potential for directing the cellular fate toward an osteogenic direction, indicated by mineralisation of transfected muscle tissue. However, a large variation in size and shape of mineralised areas was observed. Therefore, a density threshold (100 - 600 mgHA/cm<sup>3</sup>) was selected to limit areas of mineralisation for volume approximation. Potential diffusion of transfection solution could have led to this widespread effect throughout the layers of soft tissue. To prevent this, biomaterials retaining DNA complexes at the target site could be included in future experiments (Huang *et al.*, 2005; Raftery *et al.*, 2018). Also, a reduction in injection volume might decrease potential effects caused by diffusion.

To increase efficiency and concentration of transfection reagent at the desired region, another

option for improvement might be repetitive transfections (Kawai *et al.*, 2003). However, regarding ease of handling and application, as well as animal-stress reduction, single shot transfection remains the preferable approach, if possible. Finally, since the ectopic-bone model was a first step to prove the efficacy of the plasmids *in vivo*, experiments in bone defect models will be needed to evaluate their potential for clinical application. Within these models, stationary biomaterials and/or hybrid vector pre-transfected MSCs could locally contribute to stimulate mineralisation and improve bone healing.

The main concept of these plasmids is versatility. The constructs were designed to be adjustable to different target tissues using specific miRNAs with corresponding therapeutic genes, thereby providing the opportunity to meet various clinical demands.

### Conclusion

Scientific findings on miRNAs and their effects have increased in recent years. The present study contributed significantly to the field of tissue regeneration. *In vitro* validation of double-active non-viral hybrid plasmids showed increased osteoinduction in different cell lines. Acting *via* simultaneous overexpression of BMP2 and miRNAs, the plasmids not only supported the osteogenic differentiation process, but could also counterbalance the potential drawbacks of conventional gene therapy. Further refinement of invention should be pursued in the future, which could be done in a calvarial defect model. The studied constructs could also be adjusted to meet the requirements for different targets and tissues. Therefore, the presented vector system could meet the demands of a broad field of clinical applications. The present study hoped to encourage additional research on multi-target gene therapeutic approaches.

### Availability of data and material

The datasets used and/or analysed during the current study are available upon reasonable request to the corresponding author.

### Acknowledgements

We thank Matthias Hackl and Andreas Diendorfer (TAmiRNA) for the quantitation and visualisation of miRNA expression profiles, Gabriele Leinfellner for *in vivo* imaging support and Barbara Schädler, LBIT's competence centre of histology.

T.K.B. built the initial constructs, designed and performed *in vitro* experiments, analysed data and wrote the manuscript. K.P.M. designed and performed *in vivo* experiments, histology pre-processing, analysed data and wrote the manuscript. D.H. was

involved in drafting and editing of the manuscript. S.S. performed *in vitro* experiments, analysed data and edited the manuscript. P.H. performed all  $\mu$ CT scans and imaging processing. C.K. performed *in vivo* experiments and was responsible for animal care. S.N. performed and supervised the histological analysis. H.R. is the director and co-supervisor. A.H. designed and supervised the study. All authors discussed the results and implications and commented on the manuscript at all stages.

The authors declare that they have no competing interests.

### References

- Al-Dosari MS, Gao X (2009) Non-viral gene delivery: principle, limitations, and recent progress. *AAPS J* **11**: 671-681.
- Anders S, Pyl PT, Huber W (2015) HTSeq-A Python framework to work with high-throughput sequencing data. *Bioinformatics* **31**: 166-169.
- Ando H, Hirose M, Kurosawa G, Impey S, Mikoshiba K (2017) Time-lapse imaging of microRNA activity reveals the kinetics of microRNA activation in single living cells. *Sci Rep* **7**: 1-16.
- Audigé L, Griffin D, Bhandari M, Kellam J, Rüedi TP (2005) Path analysis of factors for delayed healing and nonunion in 416 operatively treated tibial shaft fractures. *Clin Orthop Relat Res* **438**: 221-232.
- Bahr SM, Borgschulte T, Kayser KJ, Lin N (2009) Using microarray technology to select housekeeping genes in Chinese hamster ovary cells. *Biotechnol Bioeng* **104**: 1041-1046.
- Bleiziffer O, Eriksson E, Yao F, Horch RE, Kneser U (2007) Gene transfer strategies in tissue engineering. *J Cell Mol Med* **11**: 206-223.
- Chen TS, Lai RC, Lee MM, Choo ABH, Lee CN, Lim SK (2009) Mesenchymal stem cell secretes microparticles enriched in pre-microRNAs. *Nucleic Acids Res* **38**: 215-224.
- Deng Y, Bi X, Zhou H, You Z, Wang Y, Gu P, Fan X (2014) Repair of critical-sized bone defects with anti-miR-31-expressing bone marrow stromal stem cells and poly(glycerol sebacate) scaffolds. *Eur Cells Mater* **27**: 13-25.
- Dimitriou R, Jones E, McGonagle D, Giannoudis PV (2011) Bone regeneration: current concepts and future directions. *BMC Med* **9**: 1-10.
- Dobin A, Davis CA, Schlesinger F, Drenkow J, Zaleski C, Jha S, Batut P, Chaisson M, Gingeras TR (2013) STAR: ultrafast universal RNA-seq aligner. *Bioinformatics* **29**: 15-21.
- Duvoisin R, Ayuk MA, Rinaldi G, Suttiprapa S, Mann VH, Lee CM, Harris N, Brindley PJ (2012) Human U6 promoter drives stronger shRNA activity than its schistosome orthologue in *Schistosoma mansoni* and human fibrosarcoma cells. *Transgenic Res* **21**: 511-521.
- Ekhteraei-Tousi S, Mohammad-Soltani B, Sadeghizadeh M, Mowla SJ avad, Parsi S, Soleimani

- M (2015) Inhibitory effect of hsa-miR-590-5p on cardiosphere-derived stem cells differentiation through downregulation of TGFB signaling. *J Cell Biochem* **116**: 179-191.
- Eliceiri K, Schneider CA, Rasband WS, Eliceiri KW (2012) NIH Image to ImageJ: 25 years of image analysis HISTORICAL commentary NIH Image to ImageJ: 25 years of image analysis. *Nat Methods* **9**: 671-675.
- Eskildsen T, Taipaleenmäki H, Stenvang J, Abdallah BM, Ditzel N, Nossent AY, Bak M, Kauppinen S, Kassem M (2011) MicroRNA-138 regulates osteogenic differentiation of human stromal (mesenchymal) stem cells *in vivo*. *Proc Natl Acad Sci USA* **108**: 6139-6144.
- Feichtinger GA, Hacobian A, Hofmann AT, Wassermann K, Zimmermann A, van Griensven M, Redl H (2014a) Constitutive and inducible co-expression systems for non-viral osteoinductive gene therapy. *Eur Cell Mater* **27**: 166-184.
- Feichtinger GA, Hofmann AT, Slezak P, Schuetzenberger S, Kaipel M, Schwartz E, Neef A, Nomikou N, Nau T, Van Griensven M, McHale AP, Redl H (2014b) Sonoporation increases therapeutic efficacy of inducible and constitutive BMP2/7 *in vivo* gene delivery. *Hum Gene Ther Methods* **25**: 57-71.
- Gámez B, Rodríguez-Carballo E, Bartrons R, Rosa JL, Ventura F (2013) MicroRNA-322 (miR-322) and its target protein Tob2 modulate osterix (Ox) mRNA stability. *J Biol Chem* **288**: 14264-14275.
- Garzon-Alvarado DA, Gutiérrez ML, Calixto LF (2014) A computational model of clavicle bone formation: a mechano-biochemical hypothesis. *Bone* **61**: 132-137.
- Glover DJ, Lipps HJ, Jans DA (2005) Towards safe, non-viral therapeutic gene expression in humans. *Nat Rev Genet* **6**: 299-310.
- Grimm D, Wang L, Lee JS, Schürmann N, Gu S, Börner K, Storm TA, Kay MA (2010) Argonaute proteins are key determinants of RNAi efficacy, toxicity, and persistence in the adult mouse liver. *J Clin Invest* **120**: 3106-3119.
- Hacobian AR, Posa-Markaryan K, Sperger S, Stainer M, Hercher D, Feichtinger GA, Schuh CM, Redl H (2016) Improved osteogenic vector for non-viral gene therapy. *Eur Cell Mater* **31**: 191-204.
- Hamberg M, Backes C, Fehlmann T, Hart M, Meder B, Meese E, Keller A (2016) MiRTargetLink—miRNAs, genes and interaction networks. *Int J Mol Sci* **17**: 1-6.
- Hampf M, Gossen M (2007) Promoter crosstalk effects on gene expression. *J Mol Biol* **365**: 911-920.
- Huang RL, Yuan Y, Tu J, Zou GM, Li Q (2014) Opposing TNF- $\beta$ - and BMP-2-activated MAPK signaling pathways converge on Runx2 to regulate BMP-2-induced osteoblastic differentiation. *Cell Death Dis* **5**: 1-11.
- Huang YC, Simmons C, Kaigler D, Rice KG, Mooney DJ (2005) Bone regeneration in a rat cranial defect with delivery of PEI-condensed plasmid DNA encoding for bone morphogenetic protein-4 (BMP-4). *Gene Ther* **12**: 418-426.
- Jackson A, Vayssière B, Garcia T, Newell W, Baron R, Roman-Roman S, Rawadi G (2005) Gene array analysis of Wnt-regulated genes in C3H10T1/2 cells. *Bone* **36**: 585-598.
- Jane JA, Dunford BA, Kron A, Pittman DD, Sasaki T, Li JZ, Li H, Alden TD, Dayoub H, Hankins GR, Kallmes DF, Helm GA (2002) Ectopic osteogenesis using adenoviral bone morphogenetic protein (BMP)-4 and BMP-6 gene transfer. *Mol Ther* **6**: 464-470.
- Karagkouni D, Paraskevopoulou MD, Chatzopoulos S, Vlachos IS, Tastsoglou S, Kanellos I, Papadimitriou D, Kavakiotis I, Maniou S, Skoufos G, Vergoulis T, Dalamagas T, Hatzigeorgiou AG (2018) DIANA-TarBase v8: a decade-long collection of experimentally supported miRNA-gene interactions. *Nucleic Acids Res* **46**: D239-D245.
- Kawai M, Bessho K, Kaihara S, Sonobe J, Oda K, Iizuka T, Maruyama H (2003) Ectopic bone formation by human bone morphogenetic protein-2 gene transfer to skeletal muscle using transcutaneous electroporation. *Hum Gene Ther* **14**: 1547-1556.
- Kay MA (2011) State-of-the-art gene-based therapies: the road ahead. *Nat Rev Genet* **12**: 316-328.
- Kempen DHR, Creemers LB, Alblas J, Lu L, Verbout AJ, Yaszemski MJ, Dhert WJA (2010) Growth factor interactions in bone regeneration. *Tissue Eng Part B Rev* **16**: 551-566.
- Koh JT, Zhao Z, Wang Z, Lewis IS, Krebsbach PH, Franceschi RT (2008) Combinatorial gene therapy with BMP2/7 enhances cranial bone regeneration. *J Dent Res* **87**: 845-849.
- Li KC, Lo SC, Sung LY, Liao YH, Chang YH, Hu YC (2017) Improved calvarial bone repair by hASCs engineered with Cre/loxP-based baculovirus conferring prolonged BMP-2 and MiR-148b co-expression. *J Tissue Eng Regen Med* **11**: 3068-3077.
- Liao YH, Chang YH, Sung LY, Li KC, Yeh CL, Yen TC, Hwang SM, Lin KJ, Hu YC (2014) Osteogenic differentiation of adipose-derived stem cells and calvarial defect repair using baculovirus-mediated co-expression of BMP-2 and miR-148b. *Biomaterials* **35**: 4901-4910.
- Lian JB, Stein GS, van Wijnen AJ, Stein JL, Hassan MQ, Gaur T, Zhang Y (2012) MicroRNA control of bone formation and homeostasis. *Nat Rev Endocrinol* **8**: 212-227.
- Lim LP, Lau NC, Garrett-Engele P, Grimson A, Schelter JM, Castle J, Bartel DP, Linsley PS, Johnson JM (2005) Microarray analysis shows that some microRNAs downregulate large numbers of target mRNAs. *Nature* **433**: 769-773.
- Linero I, Chaparro O (2014) Paracrine effect of mesenchymal stem cells derived from human adipose tissue in bone regeneration. *PLoS One* **9**: 1-12.
- Lounev VY, Ramachandran R, Wosczyzna MN, Yamamoto M, Maidment ADA, Shore EM, Glaser DL, Goldhamer DJ, Kaplan FS (2009) Identification of progenitor cells that contribute to ectopic skeletogenesis. *J Bone Joint Surg Am* **91**: 652-663.

- Love MI, Huber W, Anders S (2014) Moderated estimation of fold change and dispersion for RNA-seq data with DESeq2. *Genome Biol* **15**: 1-21.
- Luk KDK, Chen Y, Cheung KMC, Kung HF, Lu WW, Leong JCY (2003) Adeno-associated virus-mediated bone morphogenetic protein-4 gene therapy for *in vivo* bone formation. *Biochem Biophys Res Commun* **308**: 636-645.
- Maier T, Güell M, Serrano L (2009) Correlation of mRNA and protein in complex biological samples. *FEBS Lett* **583**: 3966-3973.
- Masilamani TJ, Loiselle JJ, Sutherland LC (2014) Assessment of reference genes for real-time quantitative PCR gene expression normalization during C2C12 and H9c2 skeletal muscle differentiation. *Mol Biotechnol* **56**: 329-339.
- Mingozzi F, High KA (2011) Therapeutic *in vivo* gene transfer for genetic disease using AAV: progress and challenges. *Nat Rev Genet* **12**: 341-355.
- Peng B, Chen Y, Leong KW (2015) MicroRNA delivery for regenerative medicine. *Adv Drug Deliv Rev* **88**: 108-122.
- Prowse PDH, Elliott CG, Hutter J, Hamilton DW (2013) Inhibition of Rac and ROCK signalling influence osteoblast adhesion, differentiation and mineralization on titanium topographies. *PLoS One* **8**: 17-26.
- Qureshi AT, Monroe WT, Dasa V, Gimble JM, Hayes DJ (2013) MiR-148b-nanoparticle conjugates for light mediated osteogenesis of human adipose stromal/stem cells. *Biomaterials* **34**: 7799-7810.
- Raftery RM, Mencía-Castaño I, Sperger S, Chen G, Cavanagh B, Feichtinger GA, Redl H, Hacopian A, O'Brien FJ (2018) Delivery of the improved BMP-2-advanced plasmid DNA within a gene-activated scaffold accelerates mesenchymal stem cell osteogenesis and critical size defect repair. *J Control Release* **283**: 20-31.
- Rahim MI, Weizbauer A, Evertz F, Hoffmann A, Rohde M, Glasmacher B, Windhagen H, Gross G, Seitz JM, Mueller PP (2017) Differential magnesium implant corrosion coat formation and contribution to bone bonding. *J Biomed Mater Res A* **105A**: 697-709.
- Rawadi G, Vayssière B, Dunn F, Baron R, Roman-Roman S (2003) BMP-2 controls alkaline phosphatase expression and osteoblast mineralization by a Wnt autocrine loop. *J Bone Miner Res* **18**: 1842-1853.
- Santos JL, Pandita D, Rodrigues J, Pêgo AP, Granja PL, Tomás H (2011) Non-viral gene delivery to mesenchymal stem cells: methods, strategies and application in bone tissue engineering and regeneration. *Curr Gene Ther* **11**: 46-57.
- Schindelin J, Arganda-Carreras I, Frise E, Kaynig V, Longair M, Pietzsch T, Preibisch S, Rueden C, Saalfeld S, Schmid S, Tinevez J-Y, White DJ, Hartenstein V, Eliceiri K, Tomancak P, Cardona A (2012) Fiji: an open source platform for biological image analysis. *Nat Methods* **9**: 676-682.
- Schmittgen TD, Livak KJ (2008) Analyzing real-time PCR data by the comparative CT method. *Nat Protoc* **3**: 1101-1108.
- Schoolmeesters A, Eklund T, Leake D, Vermeulen A, Smith Q, Aldred SF, Fedorov Y (2009) Functional profiling reveals critical role for miRNA in differentiation of human mesenchymal stem cells. *PLoS One* **4**: 1-9.
- Scott MA, Levi B, Askarinam A, Nguyen A, Rackohn T, Ting K, Soo C, James AW (2012) Brief review of models of ectopic bone formation. *Stem Cells Dev* **21**: 655-667.
- Shearwin KE, Callen BP, Egan JB (2005) Transcriptional interference - a crash course. **21**: 339-345.
- Sood S, Gupta S, Mahendra A (2012) Gene therapy with growth factors for periodontal tissue engineering—a review. *Med Oral Patol Oral Cir Bucal* **17**: e301-310.
- Southwood LL, Frisbie DD, Kawcak CE, McIlwraith CW (2004) Delivery of growth factors using gene therapy to enhance bone healing. *Vet Surg* **33**: 565-578.
- Stoeger T, Proetzel G, Welzel H, Papadimitriou A, Dony C, Balling R, Hofmann C (2002) In situ gene expression analysis during BMP2-induced ectopic bone formation in mice shows simultaneous endochondral and intramembranous ossification. *Growth Factors* **20**: 197-210.
- Strauss FJ, Stähli A, Kobatake R, Tangl S, Heimel P, Apaza Alccayhuaman KA, Schosserer M, Hackl M, Grillari J, Gruber R (2020) MiRNA-21 deficiency impairs alveolar socket healing in mice. *J Periodontol* **91**: 1664-167
- Umulis D, O'Connor MB, Blair SS (2009) The extracellular regulation of bone morphogenetic protein signaling. *Development* **136**: 3715-3728.
- Vasudevan S (2012) Posttranscriptional Upregulation by MicroRNAs. *Wiley Interdiscip Rev RNA* **3**: 311-330.
- Vishal M, Vimalraj S, Ajeetha R, Gokulnath M, Keerthana R, He Z, Partridge NC, Selvamurugan N (2017) MicroRNA-590-5p stabilizes Runx2 by targeting Smad7 during osteoblast differentiation. *J Cell Physiol* **232**: 371-380.
- Wang W, Li W, Ma N, Steinhoff G (2013) Non-viral gene delivery methods. *Curr Pharm Biotechnol* **14**: 46-60.
- Weilner S, Grillari-Voglauer R, Redl H, Grillari J, Nau T (2015a) The role of microRNAs in cellular senescence and age-related conditions of cartilage and bone. *Acta Orthop* **86**: 92-99.
- Weilner S, Skalicky S, Salzer B, Keider V, Wagner M, Hildner F, Gabriel C, Dovjak P, Pietschmann P, Grillari-Voglauer R, Grillari J, Hackl M (2015b) Differentially circulating miRNAs after recent osteoporotic fractures can influence osteogenic differentiation. *Bone* **79**: 43-51.
- Wilkinson L, Kolle G, Wen D, Piper M, Scott J, Little M (2003) *crim1* regulates the rate of processing and delivery of bone morphogenetic proteins to the cell surface. *J Biol Chem* **278**: 34181-34188.
- Wosczyzna MN, Biswas AA, Cogswell CA, Goldhamer DJ (2012) Multipotent progenitors

resident in the skeletal muscle interstitium exhibit robust BMP-dependent osteogenic activity and mediate heterotopic ossification. *J Bone Miner Res* **27**: 1004-1017.

Wu S, Liu W, Zhou L (2016) MiR-590-3p regulates osteogenic differentiation of human mesenchymal stem cells by regulating APC gene. *Biochem Biophys Res Commun* **478**: 1582-1587.

Yu S, Geng Q, Pan Q, Liu Z, Ding S, Xiang Q, Sun F, Wang C, Huang Y, Hong A (2016) MiR-690, a Runx2-targeted miRNA, regulates osteogenic differentiation of C2C12 myogenic progenitor cells by targeting NF-kappaB p65. *Cell Biosci* **6**: 1-14.

Zhai Y, Tyagi SC, Tyagi N (2017) Cross-talk of MicroRNA and hydrogen sulfide: a novel therapeutic approach for bone diseases. *Biomed Pharmacother* **92**: 1073-1084.

Zarecki P, Hackl M, Grillari J, Debono M, Eastell R (2020) Serum microRNAs as novel biomarkers for osteoporotic vertebral fractures. *Bone* **130**: 115105. DOI: 10.1016/j.bone.2019.115105.

Zhang J, Fu W, He M, Xie W, Lv Q, Wan G, Li G, Wang H, Lu G, Hu X, Jiang S, Li J, Lin MCM, Zhang Y, Kung H (2011) MiRNA-20a promotes osteogenic differentiation of human mesenchymal stem cells by co-regulating BMP signaling. *RNA Biol* **8**: 829-838.

Zhang Z, Xiang L, Wang Y, Jiang Y, Cheng Y, Xiao GG, Ju D, Chen Y (2020) Effect of Diosgenin on the Circulating MicroRNA Profile of Ovariectomized Rats. *Front Pharmacol* **11** : 207. DOI: 10.3389/fphar.2020.00207.

### Web References

1. <https://www.bioinformatics.babraham.ac.uk/projects/fastqc/> [25-09-2020]
2. <https://www.ncbi.nlm.nih.gov/geo/info/seq.html> [25-09-2020]
3. [http://www.targetscan.org/cgi-bin/targetscan/mmu\\_71/targetscan.cgi?mirg=mmu-miR-590-5p](http://www.targetscan.org/cgi-bin/targetscan/mmu_71/targetscan.cgi?mirg=mmu-miR-590-5p) [25-09-2020]

### Discussion with Reviewers

**Jennifer Bara:** In terms of biological mechanisms, which molecular pathways are known to be involved in BMP2-mediated muscle-bone transformation?

**Authors:** With regard to molecular signalling pathways leading to formation of ossification in muscle tissue, Kan *et al.* (2018, additional reference) suggested that aside from the TGF $\beta$ /BMP pathway, other signalling pathways, such as Wnt, the FGF and the Hedgehog pathways, may contribute by cross-talk with the central BMP pathway. Although it is not clear *via* which specific pathway ectopic mineralisation in the present *in vivo* study was induced upon transfection with the hybrid plasmid,

literature suggests that hsa-miR-590 is involved with TGFBR2 and Smad7 as well as the Wnt/beta catenin signalling pathway and can also induce osteogenic differentiation in MSCs (Ekhteraei-Tousi *et al.*, 2015; Vishal *et al.*, 201, Wu *et al.*, 2016).

**Jennifer Bara:** What advantages does this vector system confer over other viral and non-viral methods of gene delivery? Could higher levels of control, *i.e.* an inducible, tissue-specific approach be achieved using this type of hybrid vector?

**Authors:** One of the general advantages of the vector system was the non-viral base of the plasmid, which allowed for transient expression of therapeutic proteins for tissue regeneration. In contrast to viral gene therapeutic approaches, which holds a multitude of pitfalls, transient therapeutic intervention suits ideally the demands of tissue regeneration. Also, as previous work shows (Hacopian *et al.*, 2016), it is possible to overcome low target-gene expression, one major disadvantage in comparison to viral gene delivery, by combining a strong promoter as well as a codon-optimised BMP2-sequence. Furthermore, by using the combinatorial approach of BMP2 overexpression and miRNA-dependent gene regulation favouring the same result, *i.e.* pushing cell fate towards osteogenic differentiation and creating a beneficial environment for bone regeneration. Also, as endogenous cells express the introduced BMP2 directly, adequate posttranslational modifications provide more bioactivity in comparison to recombinant proteins (Brooks, 2006; additional reference).

**Jennifer Bara:** BMP2/BMP7 heterodimers are known to have more osteogenic potency when compared to homodimers. Do the authors know in which form(s) endogenous/plasmid-delivered BMP2 was present?

**Authors:** Immunohistochemistry, using anti-BMP7-antibodies, was not performed. Therefore, it is not known if delivered BMP2 was present as a homodimer or as a heterodimer together with endogenous BMP7. However, induction of endogenous BMPs can be achieved upon gene transfer with BMP2 and BMP7 (Zhu *et al.*, 2006, additional reference). Data suggested that most of the released BMP2 was present in a homodimeric state, but additional endogenous expression of other BMPs, including BMP7, probably resulted in different heterodimers. Unfortunately, there is no ELISA assay specified for detecting BMP heterodimers, such as BMP2/BMP7 dimers. The setup was focused on the evaluation of the hybrid vector system using BMP2 homodimers, but with future prospect of integrating co-expression of BMP2 and BMP7 in this system. This could further contribute to successful bone formation, as priorly shown by Feichtinger *et al.* (2014a) and Kawai *et al.* (2006) as the heterodimer would be more stable towards endogenous inhibition.

**Georg Feichtinger:** The described work tested an expression system designed using human sequences. Are there any differences in target specificity expected in a murine system for the applied miRNAs? Has the target analysis been performed on murine or human transcripts?

**Authors:** Target prediction has been performed on human transcripts, whereas, high sequence similarities exist for the used miRNAs in both organisms. Both seed sequences of hsa-miR-148b are complementary to the murine ortholog mmu-miR-148. Binding sequences for mmu-miR-148b are found in the orthologous murine *Rock1* mRNA sequence. The murine miR-590, which is complementary to the human miR-590, shares its seed sequence with mmu-miR-21a, which targets the *tgfb2*, *tgfbr1*, *crim1*, *bmpr2* and *bmpr1a* mRNAs. hsa-miR-20a shares binding sites with the murine mmu-miR-20a, these are located in the mRNA sequences of *bambi*, *bmpr2*, *crim1*, *bmpr2k*, *bmpr2*, *tgfbr2* and *smad 4-7*. All data were retrieved from mirbase.org, TarBase and ensembl.org.

**Georg Feichtinger:** Whilst the current system is interesting and relatively novel, its suitability for clinical translation could be questioned by highlighting the use of highly pleiotropic miRNAs as effectors, which could affect the expression of multiple known and unknown target transcripts. What obstacles or issues could be faced when planning to use the proposed miRNAs in human patients in the future?

**Authors:** We agree that miRNA action is pleiotropic, but also that it is considered to fine-regulate and balance homeostasis in cells and tissues. Therefore, the transient transcription of miRNAs in combination with equally pleiotropic proteins such as BMP2 might be therapeutically valuable and, indeed, several RNAi-based therapies are under clinical trials. To bring the approach closer to the clinics, safety has to be tested in pre-clinical models to exclude that the miRNAs might have an influence on a wide range of cell functions, affecting proliferation, differentiation, apoptosis and other metabolic processes by down- or up-regulating target-gene expression (Felekakis *et al.*, 2010, additional reference; Lim *et al.*, 2005; Liao *et al.*, 2014; Qureshi *et al.*, 2013; Schoolmeesters *et al.*, 2009; Vishal *et al.*, 2017, additional reference). As opposed to siRNA, complementarity between miRNA and its target mRNA does not require perfect matching. This results in an effect where one mRNA is regulated by a multitude of different miRNAs, while a single miRNA recognises multiple targets at once (Lim *et al.*, 2005), similar to the mechanism of action of transcription factors. Finally, also secretion of miRNAs into the supernatant in the *in vitro* experiments was observed, implying that systemic effects might be possible. Therefore, it needs to be carefully established whether the increased versatility of the used system, in addition to its higher efficacy, makes it safe to use.

**Georg Feichtinger:** Inclusion of miRNA cassettes into expression systems might lead to additional positional cis-acting effects that might influence gene expression of the therapeutic transgene positively or negatively and might impact therapeutic outcome indirectly. Did the authors investigate such potential effects using a control cassette or can they comment on this potential effect?

**Authors:** No, positional cis-acting effects were not investigated. Interestingly, as described in a study by Hampf *et al.* (2007), in which crosstalk signals between different promoters were investigated, the presence of the EF1 $\alpha$  promoter shows only little effect on reporter gene expression. The possibility of cis-acting effects cannot be excluded. However, the differences in miRNA effects and their impact on gene expression were shown (Fig. 5,7), including NGS data to support the study hypothesis. Therefore, we are convinced that the desired results can not only be due cis-acting contribution by the U6 promoter. As an addition, future experiments may include trials using MetLuc reporter genes to further investigate cis-acting effects.

**Georg Feichtinger:** miRNA effectors can target specific transcripts or can show a pleiotropic effect due to the regulation of multiple downstream target mRNAs. Did the authors investigate the number of target mRNAs potentially regulated by the employed miRNAs and their function in the obtained NGS data? Can they comment on the potential impact of the targeting of multiple intended and unintended target mRNAs for future translation of this technology?

**Authors:** NGS was used to investigate commonly regulated targets, pointing out significantly up-regulated and down-regulated target genes upon transfection (Fig. 8). Also, significantly down-regulated genes were identified by NGS and mapped against all miRNA-specific validated targets derived from TarBase database (Fig. 9).

According to Ishida *et al.* (2013, additional reference) the full scale of off-target effects is only known when *in vivo* studies are conducted. Interestingly, it is even suggested that due to the miRNAs modus operandi, this being a simultaneous action of small amplitude on multiple targets, the term off-target is incorrect. However, understanding the targeting of multiple unintended effectors remains a highly complex challenge for future translation into clinical application. As we were able to show on multiple levels of expression that our selected miRNAs had the desired effect, we remain optimistic that our approach will be of high interest in future projects.

### Additional References

Brooks SA (2006) Protein glycosylation in diverse cell systems: implications for modification

and analysis of recombinant proteins. *Expert Rev Proteomics* **3**: 345-359.

Felekkis K, Touvana E, Stefanou C, Deltas C (2010) MicroRNAs: a newly described class of encoded molecules that play a role in health and disease. *Hippokratia* **14**: 236-240.

Ishida M, Selaru FM (2013) MiRNA-Based Therapeutic Strategies. *Curr Pathobiol Rep* **1**: 63-70.

Kan C, Chen L, Hu Y, Ding N, Lu H, Li Y, Kessler JA, Kan L (2018) Conserved signaling pathways underlying heterotopic ossification. *Bone* **109**: 43-48.

Zhu W, Kim J, Cheng C, Rawlins BA, Boachie-Adjei O, Crystal RG, Hidaka C (2006) Noggin regulation of BMP 2/7 heterodimer activity *in vitro*. *Bone* **39**: 61-71.

**Editor's note:** The Scientific Editor responsible for this paper was Martin Stoddart.

### Supplementary video details

(available on paper website)

**Video 1. CT-generated 3D reconstruction of mouse hind limbs 8 weeks after transfection with indicated plasmids.** Transfection-induced ectopic mineralisation is shown in colour distinctly located within the soft tissue. Tibial and fibular bone is visible in white. Depicted hind limbs in the video correspond to the samples processed for histology (Fig. 12,13). Samples of high and low response to transfection were included. Upper left hind limb was transfected with luciferase control plasmid. Upper middle (high response) and upper right (low response) hind limbs were transfected with pBMP2<sub>ADV</sub> plasmid. Lower left and middle (high response), as well as lower right (low response) hind limbs were transfected with pH\_BMP2<sub>ADV</sub>590 plasmid.